
Masters Theses

Student Theses and Dissertations

2008

Friction stir form welding of aluminum structures

Kamini Ashokkumar Gupta

Follow this and additional works at: https://scholarsmine.mst.edu/masters_theses



Part of the [Materials Science and Engineering Commons](#)

Department:

Recommended Citation

Gupta, Kamini Ashokkumar, "Friction stir form welding of aluminum structures" (2008). *Masters Theses*. 5431.

https://scholarsmine.mst.edu/masters_theses/5431

This thesis is brought to you by Scholars' Mine, a service of the Missouri S&T Library and Learning Resources. This work is protected by U. S. Copyright Law. Unauthorized use including reproduction for redistribution requires the permission of the copyright holder. For more information, please contact scholarsmine@mst.edu.

**FRICTION STIR FORM WELDING
OF ALUMINUM STRUCTURES**

by

KAMINI A. GUPTA

A THESIS

**Presented to the Faculty of the Graduate School of the
MISSOURI UNIVERSITY OF SCIENCE AND TECHNOLOGY**

In Partial Fulfillment of the Requirements for the Degree

MASTER OF SCIENCE IN MATERIALS SCIENCE AND ENGINEERING

2008

Approved by

**Rajiv S. Mishra, Advisor
Ronald A. Kohser
Venkat Allada**

© 2008

Kamini A. Gupta

All Rights Reserved

PUBLICATION THESIS OPTION

This thesis consists of the following two articles that have been prepared for submission for publications as follows:

Pages 16-33 are intended for submission in the JOURNAL OF MATERIALS ENGINEERING AND PERFORMANCE.

Pages 34-53 are intended for submission to the MATERIALS AND DESIGN.

ABSTRACT

The objective of this work was to demonstrate the applicability of friction stir welding (FSW) technology in the automotive industry. Increasing fuel prices, stringent safety and emission norms are continuously striving automakers to make lightweight, fuel efficient vehicles. Automotive engineers are researching for alternate materials in order to meet weight savings targets. Use of aluminum in place of steel in a car has been increasing for making lightweight vehicles.

Conventional welding and spot welding are used as preferred joining methods by the automotive industry. However, if aluminum is used in place of steel alternate joining methods are to be researched. Due to the problems associated with the joining of aluminum with conventional welding methods, use of aluminum has been limited. Substantial amount of research has been done for the development of friction stir welding for aluminum. Joints made in aluminum using the FSW method exhibit better mechanical properties, improved fatigue life and less processing problems.

This work further analyzes the scope of the FSW method for the automotive industry. Welding of various shapes commonly used in a car is considered here. The first literature covers the FSW of partial penetration butt welds for rectangular section aluminum tubes. Mechanical property determination for these welds was also performed. The second paper demonstrates entire vehicle design considering FSW as a joining process. Finite element analysis was done for the analysis of vehicle frame performance.

ACKNOWLEDGMENTS

It is a pleasure to thank the many people who made this thesis possible. I would like to express my gratitude to my Advisor, Dr. Rajiv Mishra for his enthusiasm, support and guidance. I am sincerely thankful for the opportunity he provided me to conduct research in the upcoming and challenging area of FSW. Throughout my research period, he provided encouragement, sound advice, and lots of good ideas. I would have been lost without him.

I am grateful to my committee members, Dr. Ronald A. Kohser and Dr. Venkat Allada for their precious time and inputs towards my work. I wish to thank in addition, the members of I/UCRC program for providing me with an excellent research opportunity.

I am thankful to my many student colleagues for providing a stimulating and fun environment to learn and grow. I am especially grateful to Steven Webb and Wei Yuan for their valuable suggestions and assistance. I am also grateful to Nagarajan, Dr. Wang, Tim, Manasij, Pradeep, Harish, Saumyadeep, Prabhanjana, Abhilash, Partha, Dr. Dutta, Marco, Bharat, Gaurav and Mohan for their encouragement and moral support.

I wish to thank all my friends for their emotional support and caring. Lastly, and most importantly, I wish to thank my dearest family for their trust, support, care and love and I dedicate my thesis to my family.

TABLE OF CONTENTS

	Page
PUBLICATION THESIS OPTION.....	iii
ABSTRACT.....	iv
ACKNOWLEDGMENTS	v
LIST OF ILLUSTRATIONS.....	viii
LIST OF TABLES.....	x
SECTION	
1. INTRODUCTION.....	1
2. BACKGROUND.....	3
2.1 CLASSIFICATION OF WELDING PROCESS.....	3
2.2 MATERIAL SELECTION IN THE AUTOMOTIVE INDUSTRY.....	5
2.3 AUTOMOTIVE WELDING PROCESSES.....	7
2.4 EQUIPMENT FOR GMAW.....	8
2.5 JOINTS IN THE AUTOMOTIVE INDUSTRY.....	9
2.6 ALTERNATE JOINING METHODS.....	10
2.7 FSW VS. CONVENTIONAL WELDING.....	11
2.8 FRICTION STIR WELDING.....	12
2.9 FRICTION STIR FORM WELDING.....	13
2.10 REFERENCES.....	15
PAPER	
1. Friction Stir Welding of Rectangular 6063 Aluminum Tubes.....	16
ABSTRACT.....	16
1.1 INTRODUCTION	17
1.2 EXPERIMENTAL PROCEDURE.....	18
1.3 RESULTS AND DISCUSSION.....	19
1.3.1 Plunge Force Analysis.....	19
1.3.2 Effect of paint bake (PB) and penetration depth (PD) optimization.....	21
1.3.3 Process map development.....	23
1.3.4 Failure path.....	24

1.4 CONCLUSIONS.....	25
1.5 REFERNCES	25
2.Design of Golf Cart Frame for Friction Stir Welding.....	34
ABSTRACT	34
2.1 INTRODUCTION.....	35
2.2 METHODOLOGY	37
2.2.1 Material Selection	37
2.2.2 Geometry Selection.....	40
2.2.3 Frame Design.....	43
2.3 FINITE ELEMENT ANALYSIS.....	43
2.4 CONCLUDING REMARKS.....	47
2.5 REFERNCES	48
VITA	54

LIST OF ILLUSTRATIONS

Figure	Page
SECTION 2	
2.1. Classification of Fusion Welding Processes.....	4
2.2. Classification of Non-fusion Welding Processes.....	5
2.3. Schematic of GMAW Process.....	8
2.4. Fundamental Weld Types.....	9
2.5. Types of Weld Designs.....	10
2.6. Schematic of FSW Process.....	12
2.7. Scope of Friction Stir Form Welding.....	14
PAPER 1	
1.1. Joint Designs Possible with FSW.....	27
1.2. Tube to Tube Weld Configurations.....	27
1.3. Coupon used for Tensile Testing.....	28
1.4. Plunge Force Analysis During Tool Plunge and Traverse.....	28
1.5. Transverse Weld Section along Weld Length.....	29
1.6. Specimen Details for Weld Categories.....	29
1.7. Effect of Paint Bake on Failure Loads.....	30
1.8. Comparison of Weld Beads for Different Process Parameters.....	31
1.9. Process Map for Unsupported Tube to Tube Welds.....	32
1.10. Effect of PHI on Tensile Properties.....	32
1.11. Failure Path.....	33
PAPER 2	
2.1. Schematic Representation of FSW.....	50
2.2. Yamaha GE 16 Golf Cart.....	50
2.3. Rear Suspension Sub-frame.....	50
2.4. Beam Model for Material Index Calculation.....	50
2.5. Material Selection Chart.....	51
2.6. Rear Suspension Sub-frame Designs.....	51
2.7. Box Designs for New Sub-frame.....	52

2.8. Assembly of Box and Tube I.....	52
2.9. FEA Results for Vertical Bending Deformation Mode.....	52
2.10. FEA Results for Torsional Deformation Mode.....	53

LIST OF TABLES

Table	Page
SECTION 2	
2.1. Property Comparison between Steel and Al.....	7
PAPER 1	
1.1. Tool Geometries.....	19
1.2. Process Parameter Matrix	19
1.3. Summary of Results of Tensile Testing.....	23
PAPER 2	
2.1. Postscript for Material Selection.....	40
2.2. Geometry Selection Summary	42
2.3. Elements used for FEM	44
2.4. Material Properties used for FEM.....	45

1. INTRODUCTION

The 21st century automakers are facing fierce competition and should meet stringent government regulations to sustain their positions in market. Automotive manufacturers have to conquer challenges related to safety, emissions and fuel economy and at the same time have to improvise the vehicles with respect to customer expectation, shareholder value and profits. Due to ever-increasing fuel prices, production of vehicles with high fuel economy would help automakers to achieve their sales targets. At the same time vehicle's performance, roominess and safety should not be compromised.

Weight reduction is the path followed intensely by the automotive industry in making fuel efficient vehicles. Ever increasing fuel prices demand production of light weight vehicles. Steel has gained wide acceptance because of its optimum set of mechanical properties, ease of processing, availability, and recyclability. However, aluminum holds the potential for the replacement of steel because of its comparable properties. Equivalent steel components could be fabricated in aluminum with a considerable weight reduction. Therefore, use of aluminum in the automotive industry has increased significantly. Closure panels like hood, door, deck-lids and lift-gates have been made in aluminum by some automakers [1]. For replacing steel with aluminum it is necessary to explore joining methods that should be used. Resistance spot welding, arc welding and self-piercing rivets are used for joining steel in automotive industry. However, these technologies pose some problems when used for joining aluminum.

Friction stir welding (FSW) is a new joining method invented by The Welding Institute (TWI) in 1991 [1]. FSW is a solid state joining method in which a joint is produced without melting of the workpiece. This joining mechanism is advantageous for aluminum as joints could be produced without contamination, blowholes and porosity. Also, emission levels can be controlled because of the nature of the process. FSW could be implemented to the automotive sector if it can produce automotive joints. Another aspect is to design the vehicle considering the pros and cons of FSW as a joining method. The objective of this work is to explore the FSW method for making automotive joints.

The first paper summarizes the use of the FSW method for making partial penetration welds for hollow rectangular tubes. The second paper shows an entire design analysis when parts are to be joined with the FSW method.

2. BACKGROUND

The success rate of an economy is directly proportional to the progress of its industrial and infrastructural segments. Welding as a secondary process has played a vital role in the development of agricultural, construction, aerospace, automotive, transportation and other industrial sectors. However, there is no industry more present in the world-wide community than the automobile industry. The automobile has changed the lives, culture, and economy of the people and nations that manufacture and demand them. Ever since the late 1800s when the first modern car was invented by Benz and Daimler in Germany, the industry has grown into a billion dollar industry affecting so many aspects of our lives.

The effect of motor vehicle manufacturing on other industries is very great. The special requirements of automotive mass production have had a profound influence on the technological advances in joining technology. Automotive demands have also stimulated developments in the areas of petroleum refining, steelmaking, paint, plate-glass manufacturing, and design and development of highly specialized machine tools. The welding process is a significant joining method that has grown in synchronization with the automotive industry. Welding is defined as *a process in which materials of the same fundamental types or class are brought together and caused to join through the formation of primary (and, occasionally, secondary) chemical bonds under the combined action of heat and pressure* [2]. The welding process is primarily employed for the joining of metals and alloys. However, in certain applications welding has also been used for joining plastics and composites.

2.1 CLASSIFICATION OF WELDING PROCESS

Welding is by far the most significant technology invented by mankind. History of this technology dates back to the Iron Age and Bronze Age. However, the industrial introduction of the conventional welding method was done in the nineteenth century. Since then welding has evolved and has been applied extensively in all walks of human lives. Hence, it is necessary to understand the different upcoming welding methods and

resultant properties. Different types of welding methods are available based on the variability associated with entities joined, corresponding joining mechanism and source of energy used in the process. When melting of metals is involved in the formation of a weld joint, then it is a fusion welding process. If melting is not involved in welding then it is referred to as nonfusion welding process. Depending on the energy sources used, fusion welding processes are classified as indicated in fig. 2.1. There are three fundamental sources of energy as, chemical, mechanical and electrical. Various methods exist for the generation of these three basic energy types. Chemical energy could be generated as a result of exothermic reaction of combination of metal and oxide or metal and oxygen. Chemical energy could also be generated because of a combustion reaction between fuel and oxygen. Mechanical energy could be generated due to the conversion of work through plastic deformation of material under pressure, friction, etc. Electric energy is generated by various methods like striking an electric arc between the electrode and the workpiece, resistance (I^2R) heating of the part, induction heating, on excitation through irradiation by high energy beam as in laser welding. Classification of the nonfusion welding processes based on the energy source is indicated in fig. 2.2.

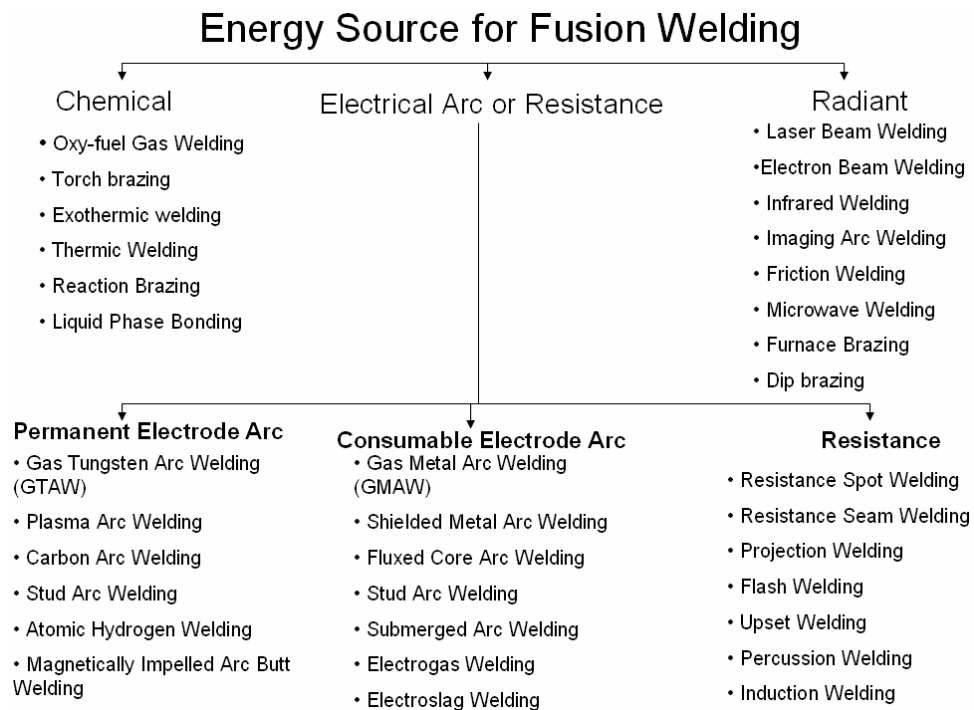


Fig. 2.1. Classification of fusion welding processes [2]

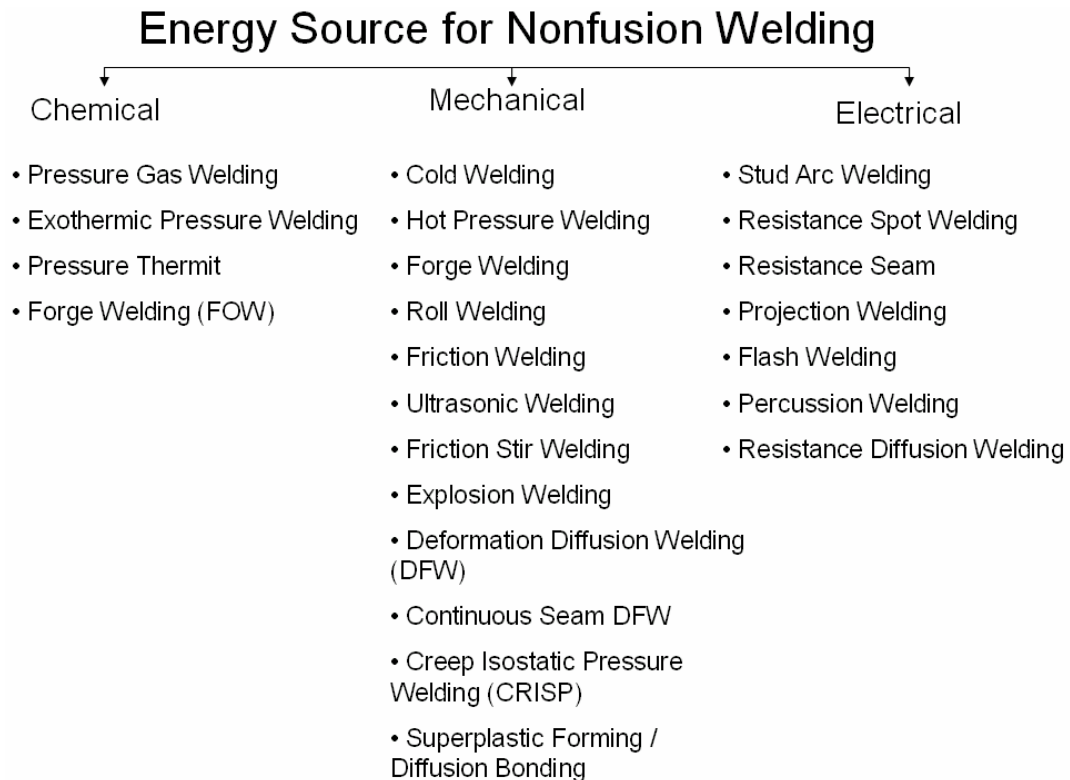


Fig. 2.2. Classification of nonfusion welding processes [2]

2.2 MATERIAL SELECTION IN THE AUTOMOTIVE INDUSTRY

The automotive industry has always been on a weight reduction program for the vehicles. A light-weight vehicle is desired because of the ever increasing fuel prices and stringent emission standards. Body-in-white (BIW) of a vehicle contributes to approximately one third of its total weight. If BIW is light then drive-train and other engine components would also be lighter, thereby weight loss targets for the vehicle could be achieved. Design engineers could use two approaches for achieving this goal:

- Vehicle downsizing, and
- Use of low density materials.

Use of low density materials and exploration of the joining methods for the same is considered here. Prior to the realization of the importance of light-weight vehicles, steels were primarily used in the fabrication of entire BIW. Steel is used in car manufacturing as it provides an optimum combination of mechanical properties,

weldability, cost, damping characteristics, crashworthiness and recyclability. MIG welding method and resistance spot welding methods are used in the fabrication of BIW. Some of the important factors on which material selection is based for the automotive industry are explained below:

Crashworthiness – It is the ability of a structure to protect its occupants during an impact. Crashworthiness of a vehicle could be determined by using computer models or experiments. Crashworthiness is assessed using parameters like the deformation pattern of the structure, deceleration experienced by the vehicle during an impact, and injury probability.

Damping Resistance – It is the resistance of the structure against the vibrations experienced by the vehicle. Due to motion of the vehicle on uneven surfaces and also because of vehicle acceleration it gets subjected to vibrations. Components on a car should sustain the fatigue cycles because of the dynamic loading due to the vibrations.

Extrudability – It is the property of material to get readily formed from a block to shapes of complex cross section by the application of large force. Variable thicknesses along length and complex cross section are abundantly used in automobiles for reducing the part counts and for the weight reduction purpose. These geometrical features are possible by performing hydroforming on the extruded part provided the part material has high extrudability index.

Weldability – It is the capacity of a material to be welded under the imposed fabrication conditions into a specific suitably designed structure and to perform satisfactorily in the intended service. Since, welding is the primary joining process for the automotive industry, it is mandatory for the material used to exhibit good weldability. This qualitative property is assessed by either direct test or indirect test [2]. Direct weldability tests make use of an actual welded sample, whereas in indirect testing the weld zone is simulated by subjecting the material to a simulated weld thermal cycle. The simulated weld zone is then analyzed for its resultant properties.

In order to reduce the vehicle weight, it is necessary to explore other materials that have lower density than steel and are abundant. This line of thought directed designers and automotive engineer's attention to the incorporation of aluminum and plastics in a car. Car designers applied a materials-substitution approach to interior components such as instrument panels, which are now almost universally made of plastic. Continuous efforts have been made for the replacement of steel with aluminum in BIW. A detailed comparison between the properties of these two metals is presented in Table 2.1. Characteristics that are particularly significant for the automotives are considered for the comparative study.

Table 2.1. Property comparison between steel and aluminum [3]

Parameter	Aluminum 6061-T6	Steel A36
Density	2.7 gm/cc	7.1 gm/cc
Corrosion resistance	Good	Fair
Weldability	Fair, but reduces strength	Good, no strength reduction
Extrudability	Very good	Not practical
Yield Strength	241 MPa	248 -345 MPa
Modulus of Elasticity	68.9 GPa	200 GPa
Elongation	8 % - 10 %	20 %
Fatigue Strength (For 5 million cycles)	70.3 MPa	165.5 MPa
Strength to weight ratio	2.8	1.0 to 1.4
Cost by Weight	\$1.20/lb	\$0.3/lb

2.3 AUTOMOTIVE WELDING PROCESSES

Spot welding and arc welding are the two most abundantly used welding processes in the automotive industry for steels. Current research work is focused on continuous welds used in a vehicle, which is arc welding. It is a fusion welding process in which an electric arc is used as a source of heat. The most commonly used arc welding process is gas metal arc welding (GMAW). It is the most popular and dominating process

amongst the fabricators. In spite of sixty years of history, research continues in this field for further improvements and developments. GMAW is commonly identified as metal inert gas (MIG) welding. GMAW has been successfully applied to a range of metals including carbon steel, stainless steel, aluminum, magnesium, copper, nickel, silicon and bronze. The GMAW process lends itself to semi-automatic, and robotic automation welding applications. GMAW, by definition is as an arc welding process which produces the coalescence of metals by heating them with an arc between a continuously fed filler metal electrode and the workpiece. Molten weld metal produced is protected by shielding it with an externally supplied gas. A potential field is created between the electrode and the workpiece which are oppositely charged. The arc consists of thermally emitted electrons and positive ions from the shielding gas. The kinetic energy of the electron is converted to heat because of its collision with the oppositely charged particles. A schematic of GMAW is indicated in fig. 2.3.

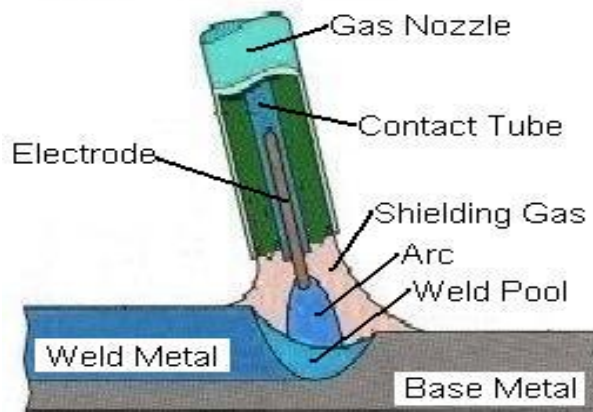


Fig. 2.3. Schematic of GMAW process [4]

2.4 EQUIPMENT FOR GMAW

There are four components involved in the industrial equipment for GMAW:

1. Power source – Combined power source and wire feed accessories are available for the current capacity range of 135-650 amps [4].
2. Wire drives and accessories - GMAW wire drive designs provide for the use of a wide range of solid or metal cored electrodes ranging from 0.6 mm – 1.6 mm in diameter. Standard wire feed mechanisms at the speed of 2 – 20 m/min. are available [4].

3. GMAW gun and cable assembly designed to deliver the shielding gas and electrode arc
4. Shielding gas apparatus and accessories – Inert shielding gases of argon and helium are used either independently or as a mixture. Reactive shielding gases like oxygen, hydrogen, nitrogen and carbon dioxide are also used

Each of the above mentioned components are selected taking into consideration a myriad of factors like the metal type that is getting joined, material thickness, joint type, the weld position, cost, etc.

2.5 JOINTS IN THE AUTOMOTIVE INDUSTRY

Geometrical constraints of the structure and the type of loading determine the type of the joint. There are four fundamental joint types as Butt (groove), fillet, plug and surfacing [2]. These are shown in fig. 2.4. Groove, fillet and plug welds are used for joining of structures, however surfacing is used for applying material to a workpiece by welding for the purpose of providing protection from wear or corrosion. Broadly, there are five joint designs that are used for generating a structure and are indicated in fig. 2.5 [2]. Other than the joint geometry, locations of the joint in the structure, accessibility, and welding process also have an influence on the joint configuration. Structures are welded using combinations of the five basic joint designs.

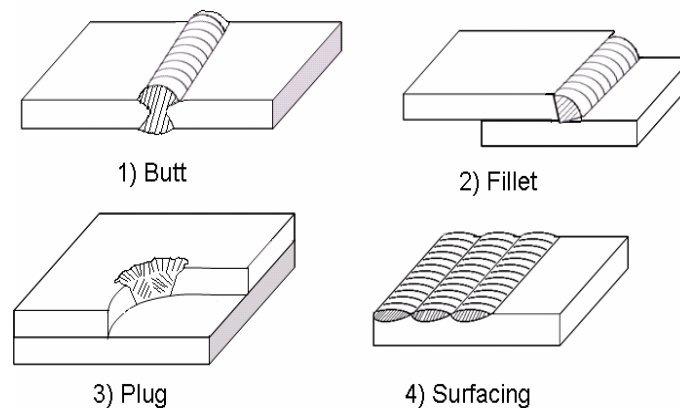


Fig. 2.4. Fundamental Weld Types [2]

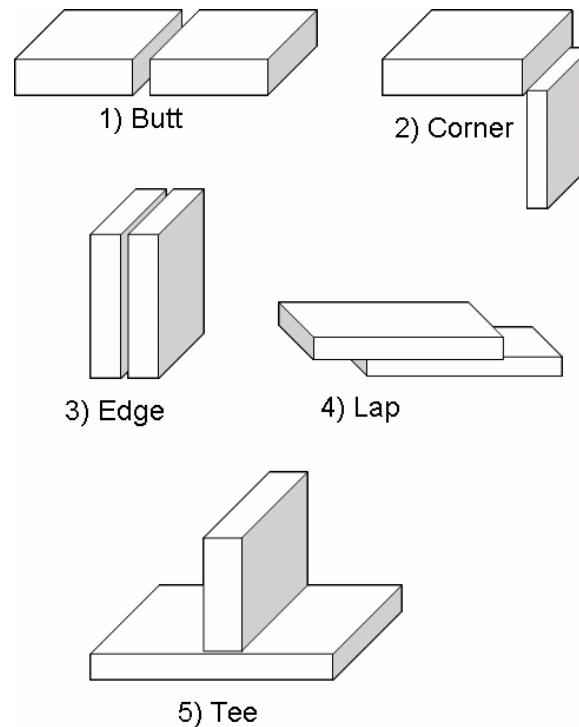


Fig. 2.5. Types of Weld Designs [2]

Joints used in an automobile are one of the five joint designs. Most of the joints in BIW are plug welds. Thousands of plug weld are used as spot welds for integrating sheet metal in the door and body of the car. The frame of the vehicle is put together by using a series of corner, lap, edge and tee joints. Exhaust pipes and mufflers in the exhaust system of the vehicle are joined by butt joints. Short continuous tee joints and lap joint are used for welding various components to the rails in the chassis.

2.6 ALTERNATE JOINING METHODS

Conventional arc welding has been established as a simple process with portable and inexpensive equipment. It is a versatile process and could be used for fabrication, assembly, maintenance, or repair, for both in-plant and field locations. Despite this there are disadvantages associated with the process. Joints are created by local melting and subsequent solidification of the molten metal. Shielding of molten metal is required to prevent contamination of the molten metal. In addition to shielding gas, expensive

consumables and filler metal are used during the process. Solidification of the molten metal at an incorrect cooling rate could produce defective welds. Cracks, porosity and contamination are some of the commonly observed weld defects in conventionally welded structures. Conventional welding consumes high amounts of energy for the melting of metals. Hazardous emissions containing hexa-valent chromium, manganese and copper are produced due to the melting of ferrous alloys during welding.

Aluminum has become the material of choice in automotive industry for accomplishing weight savings targets. Alternate welding methods are required if steel is replaced with aluminum. Joining of aluminum is possible by the GMAW method; however other welding methods could produce the same joint at a lower cost. Friction stir welding (FSW) has evolved as a significant joining method for aluminum.

2.7 FSW VS. CONVENTIONAL WELDING

FSW is a significant replacement welding method for conventional welding. FSW is a green technology producing superior joints in aluminum, steel, nickel, copper, magnesium and titanium alloys. FSW has evolved significantly over the last decade and a half. The scope for the implementation of FSW has been realized by the industrialists due to its several advantages over conventional welding methods. FSW joints are not only superior metallurgically but are produced in an environment friendly way that offers energy savings.

Weld preparation required for FSW is lower than conventional welding. Degreasing and surface cleaning requirements are not as stringent. Also, shielding gas and filler materials are not needed for FSW. It has been predicted by FSW researchers that emissions level and energy consumption would enormously come down by the application of FSW in industries [1]. FSW joints have higher strength, better fatigue life, lower distortion, less residual stress and better corrosion resistance. There is no loss of alloying elements and no undesirable changes in the different weld zones after FSW.

Though FSW has many advantages over conventional welding method, it has not matured to a point where it could be directly taken up by industries. Industrial use of conventional welding has grown over 60 years. Detailed industrial standards and specifications are available for conventional welding methods. Guidelines are defined for process, equipment, joint testing, welder education, maintenance and more for every aspect of conventional arc welding. FSW is a comparatively new technology and there are various hurdles for its industrial implementation. In broad terms, unavailability of design guidelines, welding knowledge and skills, process specification and high capital investment have slowed the industrial applicability of this welding method.

2.8 FRICTION STIR WELDING

Friction stir welding (FSW) is a solid state joining process that involves plunging and traversing a rotating non-consumable tool along the weld line. The tool used for FSW has two parts, a pin and a shoulder [1]. The pin plunges into the material that is being welded and generates frictional heat and deformational heat that softens the material. The shoulder is responsible to constrain the flow of plasticized material and to expand the softened material zone. A schematic of the FSW method is indicated in fig. 2.6.

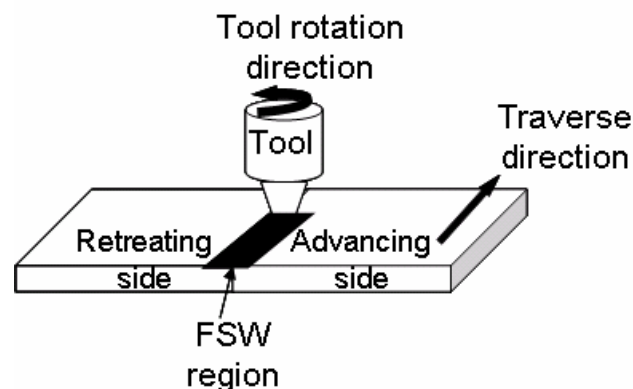


Fig. 2.6. Schematic of FSW process

For using FSW in the auto industry, it is necessary to explore it for producing various automotive joints. Both partial penetration and full penetration joints are used along with continuous and stitch weld types. Welding of different shapes, different

product forms in different orientations is desired. Some joint types involve hollow components. Also, automization is a dominating factor as it governs the productivity. The various joint types possible by FSW are butt, lap, T-butt, and fillet [1]. However, these joints are made on a laboratory scale without considering the actual manufacturing atmosphere.

FSW is associated with torques and forces because of the plunge of a tool in solid material. Hence, a suitable clamping and fixturing arrangement is required to prevent material movement during FSW. In welding of hollow components without internal support, these forces and torques need to be adequately controlled to prevent deformation. Force acting in the downward z-direction would govern the extent of tube deformation. Machine heads used in robots are also sensitive to these forces. For the purpose of automation and to prevent material deformation, plunge forces should be controlled. At the same time, complex geometries should be joined to produce required structural integrity irrespective of tool accessibility, clamping, fixture and envelope constraint issues.

2.9 FRICTION STIR FORM WELDING

Form welding refers to the welding of different shapes using the FSW method. In form welding, process optimization for welding different shapes is considered. Welding of c-channel to sheet, tube to tube, tube to sheet, and angle to sheet represent possible automotive joint types. These categories were selected based on commonly available extruded sections in aluminum. The scope of present work is to generate a catalog which includes details of different joints that are possible using FSW. Various types of joints used in automotive industries will be included in the catalog. The catalog would contain information about the part geometry, joint type, optimum tool design for a given joint, maximum permissible strength of the joint for optimized tool & process parameters and fatigue strength of the joints. This catalog would be a readily available record for the designers when parts are designed for FSW. Fig. 2.7 indicates the possible scope for friction stir form welding.

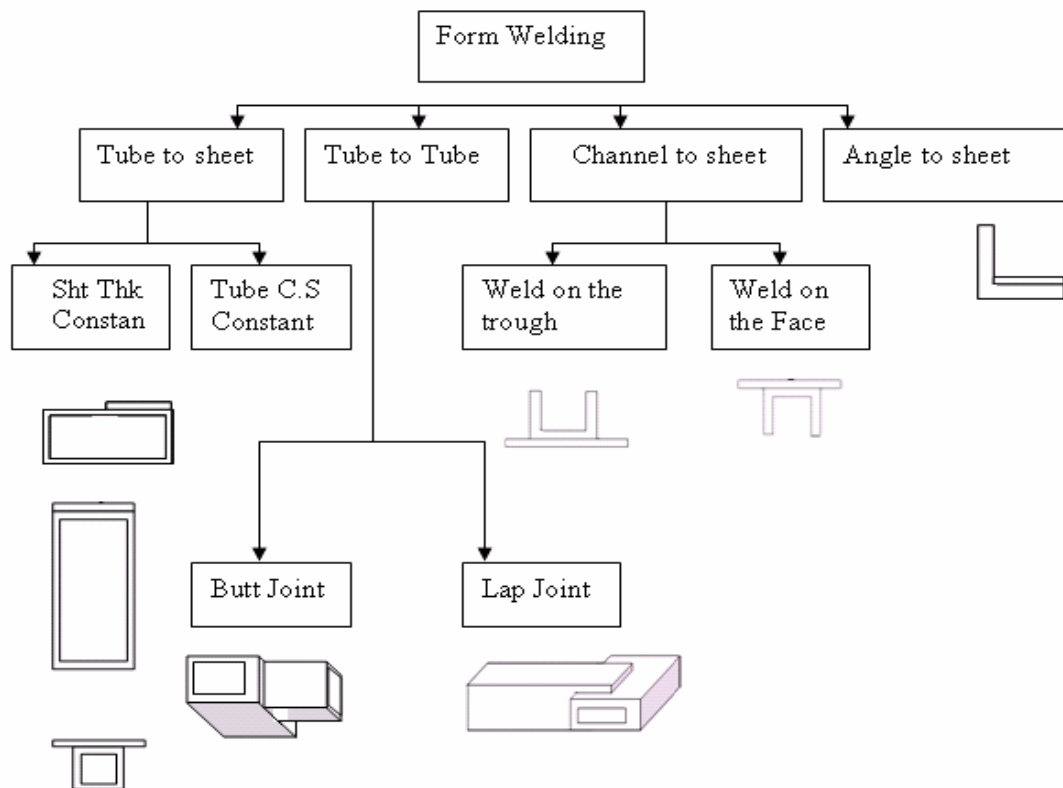


Fig. 2.7. Scope of Friction Stir Form Welding

2.10 REFERENCES

1. R. S. Mishra, M. W. Mahoney, *Friction Stir Welding and Processing, ASM International, 2007*
2. Robert. W. Messler, Jr., *Principles of Welding – Process, Physics, Chemistry and Metallurgy, Physics Textbook, Wiley-VCH, 1999*
3. J. Randolph Kissell and Robert L. Ferry, *Aluminum Structures – A Guide to their Specifications and Design, John Wiley & Sons INC., Second Edition (2002)*
4. <http://www.lincolnelectric.com>., GMAW Welding guide
5. W. J. Arbegast, “Friction Stir Welding: After a Decade of Development” , *Friction Stir Welding and Processing IV, Edited by Mishra, Mahoney, Lienert & Jata TMS (2007)*
6. Steve Lampman, Grace M. Davidson, Cheryl L. Powers, *Weld Integrity and Performance, ASM International, 1997*

PAPER**1. Friction Stir Welding of Rectangular 6063 Aluminum Tubes**

Kamini Gupta, Rajiv S. Mishra*

Department of Materials Science and Engineering

Missouri University of Science & Technology

Rolla, MO 65409, USA.

* Corresponding author: Tel.: +01 573 341 6361 fax: +01 573 341 6934

E-mail: rsmishra@mst.edu

(Prepared for submission in JOURNAL OF MATERIALS ENGINEERING AND PERFORMANCE)

ABSTRACT

The objective of the present study was to establish the feasibility of making friction stir welds (FSW) for rectangular hollow tubes. Partial Penetration welds were made for 6063 Al tubes having rectangular cross sections. FSW runs were made on a conventional machine as well as on robotic machine. A comparative study was made between unsupported and plug supported welds. Tool plunge force variation was analyzed for the weld types. Multiple weld cross sections were taken across the weld length to correlate the exerted plunge force with the tube deformation. Penetration depth (PD) was optimized for both the weld categories. Also, the effect of paint bake cycle was studied on the load bearing capability of the welds. Unsupported welds exhibited higher load bearing capability than plug supported welds. Overall joint efficiency was higher for the paint bake condition. A penetration depth of 56% gave higher failure loads for both the weld types in as-welded as well as in paint bake conditions. Optimum heat input required for the weld was quantified by developing a process map. This was done for unsupported welds on a robotic welding machine. The unsupported weld was used as it was better than plug supported weld. Runs made on the robotic machine were more uniform with respect to their load bearing capabilities. A discussion on the failure mode for two different weld types is included.

Keywords: Unsupported weld, Plug supported, Process map

1.1 INTRODUCTION

Friction stir welding is a solid state joining process that involves plunging and traversing a rotating tool along the weld line. Improved weld quality, low power requirements, no filler material, no shielding gas, and environmental friendliness are some of the significant advantages that FSW has to offer over conventional welding technology [1,2]. Industrial implementation of FSW technology is hindered because of lack of industry standards, design guidelines and design allowable [1,3]. Design for manufacturing (DFM) issue related to the fabrication of built-up structures by FSW method are addressed to some extent in the development of an aluminum rail car hopper [1,4]. Fixturing issues, process parameter optimization and design modification for FSW are considered thoroughly for the fabrication of built-up beam assemblies [5].

Aerospace and automotive industries have focused on the development of various aspects of FSW [6]. Applicability of this technology to automotive industries primarily depends on the types of the joints possible. The variety of joint designs possible by FSW are full penetration and partial penetration butt joints, lap joints [7], fillet joints, edge joints etc. and are indicated in fig. 1.1 [1,2]. These joint designs are explored for solid components where the workpiece is supported by a backing plate during the weld.

There is not much literature on the FSW of hollow structures. This work focused on exploring the possibility of joining hollow structures using FSW technique. The possibility of making partial penetration butt welds with hollow tubes was explored. Such a joint is observed mostly in vehicle frames. The forces experienced by the workpiece during welding should be kept as low as possible to minimize tube distortion. Plunge force in the downward direction which governs the deformation of hollow structure was studied. A method to control the tube distortion was explored in which a plug was used as a backing piece. Performance of the welds is analyzed in as-welded (AW) and in paint bake (PB) conditions. FSW runs were successfully made on conventional and also on the robotic machine thereby exploring the feasibility of industrial implementation.

The effect of process parameters on the weld quality was determined for process parameter optimization. The temperature attained by the workpiece during FSW affects the quality of the weld. The amount of heat input into the workpiece during FSW depends on the process parameters and could be measured by pseudo heat index (PHI) defined as below [8]:

$$PHI = \frac{rpm^2}{ipm \times 10000} \quad (1.1)$$

where, rpm is the tool rotation speed in revolutions per minute, and ipm is the tool traverse rate in inches per minute

1.2 EXPERIMENTAL PROCEDURE

Rectangular tubes of 6063 T56 Al were welded in two configurations indicated in fig. 1.2. The tubes welded were 76.2mm X 25.4mm in cross section with thickness of 3.175 mm. Single pass welds were made of 64.8mm in length each. Two welds were made, one on each horizontal surface of the joint. Plugs were machined from 3.175 mm thick plate of 6061 T6 Al alloy. Z-forces experienced by the tool while making welds on a conventional machine were recorded and analyzed for both the weld types. Z-forces were correlated with the macrostructural variations along the weld length. The first objective was to optimize the penetration depth (PD) for unsupported and plug supported welds. Welds for penetration depth optimization were made on a conventional FSW machine. For penetration depth optimization, other process variables were kept constant. These runs were made with tool rotation speed of 12.5 Hz, tool traverse rate of 1.058 mm/sec and tool tilt angle of 2.5°. Two different tools were used with two different pin heights targeting for 56% and 67% penetration of the total thickness.

All the welds were made using tools with conical stepped pin and concave shoulder. Tool geometries used are summarized in Table 1.1. FSW runs were made for 56% and 67% penetration depth for both unsupported and plug supported tubes. For both the penetration depths used, effect of paint bake cycle on failure load was determined.

Fig. 1.3 indicates the geometry of the coupon that was used for tensile testing. An MTS frame with 99 kN load capacity was used for tensile testing. All coupons were subjected to pulling in tensile mode at the rate of 0.02 mm/sec till yielding and beyond, with pulling being performed at the rate of 1 mm/sec. These coupons were subjected to the paint bake cycle at 175 °C for 30 min. A process map was developed for the unsupported weld type. Runs for development of the process map were made on the ABB robotic machine. For these runs a constant penetration depth of 1.4 mm was used with tool tilt angle of 3° and work angle of 2°. The process parameter matrix used in making the runs is indicated in Table 1.2. The effect of process parameters on failure load was also studied. Transverse weld sections were taken at different distances starting from the weld beginning. Keller's reagent was used as the etching reagent.

Table 1.1. Tool geometries

Penetration Depth %	Pin Height mm	Pin Diameter mm	Shoulder Diameter mm
67	2.1	4	12
56	1.5	4	12

Table 1.2. Process Parameter Matrix

Tool Traverse Speed mm/sec (IPM)	Tool Rotation Speed Hz (RPM)
0.423, 1.058, 2.12	12.5, 15, 16.7

1.3 RESULTS AND DISCUSSION

1.3.1 Plunge force analysis

The plunge forces varied during the weld because runs were made in position control mode. Variations in the Z-force during the tool plunge and tool traverse stages are indicated in fig. 1.4a and fig. 1.4b respectively. For this analysis unsupported and plug supported welds made for 56% PD were considered. During the tool plunge stage, with the vertical progression of the tool into the workpiece, the Z-forces increase. Maximum

Z-force during plunge was recorded as 4.72 kN for unsupported weld and 6.45 kN for plug weld. As the tool plunges into the material to reach the commanded target depth, the tool has to overcome higher material resistance in order to continue its rotation. Z-force is maximum when the tool shoulder comes in contact with the material surface. This leads to the increase in Z-force during plunge.

Temperature increase is observed by the workpiece due to the heat generated as a result of extensive plastic deformation of the material and frictional heat between the tool and the workpiece during weld. This leads to the drop in the Z-force during traverse. Z-forces during traverse drop from 5.34 kN to 3.11 kN for plug weld and from 4.45 kN to 2.67 kN for unsupported welds as the tool moves along the weld line. Average Z-force experienced by the tool during traverse was recorded as 3.93 kN for plug welds and 2.95 kN for unsupported welds. For plug welds traverse Z-forces decreases continuously along the length of the weld. For unsupported welds, traverse Z-force first decreases from the weld start (4.45 kN) to the middle of the weld length (2.67 kN) beyond which a marginal increase in the Z-force is observed towards the end (2.9 kN). Welds made on the unsupported tubes correspond to the case in which point loads act on the span of a simply supported beam. Deflection of the beam is maximum at the center and minimum at the ends. The shape of the Z-force curve follows the similar trend. However, forces at the beginning and at the end are not same. This could be because of the high temperature attained by the workpiece during the run, which causes the softening of the material.

Transverse weld sections were taken at different distances from the weld start. Locations on the weld line from where the weld cross sections were cut are indicated in fig. 1.5a Fig. 1.5b and fig. 1.5c represent transverse weld sections for unsupported and plug welds respectively. From fig. 1.4b it was noticed that the bending of the advancing side and the retreating side tubes was more at the center than at the ends. However, no bend could be seen in the weld cross section taken across the center of the weld line on the advancing side. However, bending could be seen on the retreating side. Retreating side tube has deformed to its maximum at the center. This is evident from the level mismatch observed between the two tubes. Transverse weld sections for plug welds at

different distances along the weld length are indicated in fig. 1.5c. Bending of the tube on the retreating side is minimized because of the support provided through the plug. Tube bending on the advancing side decreases along the weld length. This is in response to the Z-forces which decrease continuously along the weld length for plug supported welds.

1.3.2 Effect of paint bake (PB) and penetration depth (PD) optimization

For penetration depth optimization, all other process variables like tool rotation speed, tool traverse rate, and tool tilt angle were kept constant. The nomenclature used for different samples is indicated in fig. 1.6. Each coupon was one inch wide and the load bearing cross section area was decided based on the penetration depth used for the weld. Figs. 1.7(a-d) indicate the effects of paint bake cycle on the load bearing capabilities of the welds for the two different penetrations of 56% and 67% of the total thickness under tensile loading condition.

Fig. 1.7a illustrates the effect of paint bake cycle on sample no. 2_I for plug and unsupported welds made for 56% and 67% penetration depth. In AW condition, unsupported welds exhibit higher load bearing capability with 56% penetration depth. However, plug supported welds can withstand higher loads with 67% penetration depth than 56% penetration depth in AW condition. As expected, paint bake increases the load bearing capability for 56% penetration depth plug supported weld, 67% penetration depth plug supported weld and 56% penetration depth unsupported weld. For the 67% penetration depth unsupported weld, the effect of paint bake is not as expected. Insertion of plug was done with the hypothesis of increasing the nugget and providing support to prevent tube sagging. It was expected that plug insertion would increase the load bearing capability of the weld.

Minimum tensile load obtained for a coupon would be the load bearing capability for the entire weld length. Maximum load bearing capabilities for all welds made during this study are summarized in Table 1.3. Plug supported welds show lower load bearing capability than unsupported welds both in AW and in PB conditions. This might be because the material of the plug is different than the tube material and FSW of dissimilar

welds exhibits lower strength as compared to similar metal weld. Different studies done to analyze the effect of paint bake on the properties of FSW 6XXX series Al alloys indicate an improvement in weld strength after paint bake. Results obtained do not agree with the results of the earlier studies [1]. However, in our study we are comparing weld strengths of two different samples. If we could analyze the same coupon in AW condition and in PB conditions, different result might be expected.

Analysis of failure load against % penetration curves indicates that there is no regularity in the data for different samples. There might be some internal variations in the weld quality all along the weld length. This could be responsible for the randomness in the results of the tensile testing. Overall weld efficiency was determined for different weld types as indicated in Table 1.3. Minimum weld efficiency of 66% was recorded for optimum penetration depth of 56% for unsupported welds. The unsupported weld exhibited higher weld efficiency than plug supported weld. Welds subjected to PB treatment showed higher overall weld efficiency than AW condition.

Table 1.3. Summary of results of tensile testing

Weld Type	% Penetration	Condition	Failure Load (kN)					% Weld Efficiency
			1_I	1_II	2_I	2_II	Minimum	
TT	56	As Welded (AW)	7.7	7.1	6.05	5.95	5.95	65.88
		Paint Bake (PB)	6.35	7.55	7.9	7.6	6.35	70.30
	67	As Welded (AW)	5.6	7.6	3.5 (Unbonded Area + SLOF)	6.25	5.6	52.29
		Paint Bake (PB)	6.8	6.75	2.4 (SLOF)	2.65 (SLOF)	6.75	63.03
TTP	56	As Welded (AW)	3.55	4.75	4.4	5.4	3.55	39.30
		Paint Bake (PB)	5	5.3	4.75	5.6	4.75	52.59
	67	As Welded (AW)	Traverse TD X	Traverse TD X	5	6.3	5	46.13
		Paint Bake (PB)	5.4	6.4	5.55	6.2	5.4	49.82

1.3.3 Process map development

Visual inspection of the weld length was done for each tool rotation and tool traverse combination. These results are indicated in figs. 1.8(a-j). Scratch marks observed on some welds are because of the filing of flashes to facilitate the weld on the second side.

All welds are free from wormholes. A significant digging of the material was observed on the advancing side. Material on the retreating side had bent during the weld due to lack of support. The advancing side was supported by the tube wall. The difference in the support on advancing and retreating sides was responsible for material dig on advancing side. This extra material moved with the tool and was deposited on the retreating side. Material deposition was higher for higher heat indices as can be seen in fig. 1.8a and fig. 1.8d. Full cup was observed at all the tool rotation rate – tool traverse rate combinations. Shoulder-workpiece contact on the retreating side was not observed during the middle of the weld length for heat indices values less than 40. For almost similar heat index values of 32.4 and 36 the appearance of the weld was different as observed in fig. 1.8e and 1.8j, respectively. The PHI term defined in eqn. (1.1) does not encompass all the process variables that control heat input in the weld. Some other parameters could also be responsible for this variation, like tool geometry, clamping, temperature of the backing piece during the run, etc.

Fig. 1.9 presents the transverse weld sections for the welds indicated in fig. 1.8. The tool rotation rate-traverse rate combination of 16.7:0.423 represents the hottest weld and 12.5:2.12 represents the coldest weld made. The weld section for 16.7:0.423 tool rotation tool traverse combination was bent during cutting. The first parameter for comparison is the bending of the tube on the retreating side. Bending of retreating side tube was higher for hotter welds (16.7:0.423, 16.7:1.058 and 16.7:2.12). Within the nugget region, an arm indicating microstructural variation is observed on the advancing side for some heat indices. PHI of 100, 56.25, and 40 showed presence of this microstructurally distinct region in the nugget. Relatively colder welds for PHI of 32.4, 22.5, 16.2 and 11.25 showed a nugget which was macroscopically uniform.

Two samples were subjected to tensile testing. Samples used were as per fig. 1.3. Sample no I was taken from the end of the weld length and sample no. II was from the middle of the weld length. Failure load for these coupons was plotted against the corresponding PHI. All other parameters were kept constant. Results of tensile testing are indicated in fig. 1.10a for sample I and in fig. 1.10b for sample II respectively. PHI varied in the range of 11-100. For sample I, failure load varied from 5 kN to 7.7 kN for various heat indices. Minimum failure load of 5.3 kN was obtained for sample I for a colder weld corresponding to 11.25 PHI. For same PHI, sample II failed at a load of 6.4 kN.

Welds made on the robotic machine exhibited much less variation in load bearing capability than the welds made on the conventional machine. Heat index values in the range of 15-40 showed higher failure loads for both samples I and II respectively and exhibits a optimized process parameter window for these welds. PHI of 100 also gave failure loads of the same order as heat indices in the range of 15-40.

1.3.4 Failure path

The observed failure paths for unsupported and plug supported weld coupons when subjected to tensile loading are indicated in fig. 1.11. In both cases, failure occurred by the propagation of crack on the retreating side. Partial penetration butt welds were made as we are joining hollow structures. In the joint, partially welded thickness acts as the weakest load bearing cross section. When load is applied, the gap between two tubes continued to widen with consequent thinning of the welded area along the indicated line. This crack propagated from bottom to the top surface. For the plug supported weld, a crack initiated on the retreating side at the interface between the plug and retreating side tube. The sample was able to withstand the applied load till the critical thickness was reached, beyond which the sample failed.

1.4 CONCLUSIONS

The FSW method could be successfully used for making partial penetration butt welds for rectangular 6063 Al tubes. However, unsupported welds exhibited better

performance than plug supported welds. Difference in the material composition between the plug and the tube could be responsible for poor performance of plug-supported welds in comparison to unsupported welds. An FSW joint was possible for both unsupported and plug supported tubes. The plunge force pattern was different for unsupported and plug supported weld corresponding to the nature of the backing plate. A paint bake cycle improved overall performance of the weld. A stray randomness was observed in tensile properties of samples taken along the same weld length with same process parameters. Performance of the weld is independent of the intrinsic material properties. Welds made for 56 % target depth exhibited better properties for both the weld types. Maximum weld efficiency of around 70% was obtained for unsupported welds. Macroscopically defect free welds were possible on both a conventional and robotic welding machine, thereby demonstrating feasibility for industrial implementation. Process parameters corresponding to the PHI values in the range of 15-40 gave optimized weld performance. Samples failed on the retreating side of the weld by gradual decrease in the thickness of the region of partial penetration weld.

1.5 REFERENCES

1. R. S. Mishra, M. W. Mahoney, *Friction Stir Welding and Processing, ASM International, 2007, Chapters 1, 2, 13, and 15.*
2. C. B. Smith, J. F. Hinrichs and P. C. Ruehl, “Friction Stir and Friction Stir Spot Welding-Lean, Mean and Green”, *Friction Stir Link, Inc. W227 N546 Westmound Dr., Waukesha, WI 53186*, p.1-8.
3. W. J. Arbegast, “Friction Stir Welding: After a Decade of Development”, *Friction Stir Welding and Processing IV, Edited by Mishra, Mahoney, Lienert & Jata TMS (2007)*, p.3-17.
4. C. Allen, C. Oberembt, W. J. Arbegast, D. Medlin and H. Mercer, “Friction Stir Welding of an Aluminum Coal Hopper Railcar” , *Friction Stir Welding and Processing IV, Edited by Mishra, Mahoney, Lienert & Jata TMS (2007)*, p.19-28.

5. W. J. Arbegast and A. K. Patnaik, "Process Parameter Development and Fixturing Issues for Friction Stir Welding of Aluminum Beam Assemblies" , *SAE International* (2005)
6. A. Scafe, A. Joaquin, "Friction Stir Welding of Extruded Aluminum for Automotive Applications" , *SAE International* (2004)
7. L. Cederqvist and A. P. Reynolds, " Factors Affecting the Properties of Friction Stir Welded Aluminum Lap Joints", *Proceedings of the second international conference on Friction Stir Welding, The Welding Institute (TWI), Gothenburg, Sweden, June 2000.*
8. S. Kandukuri, W. J. Arbegast, A. K. Patnaik, and C. D. Allen, "Development of Design Curves for Tensile Strength and Fatigue Characteristics of 7075 T73 Aluminum FSW Butt Joints" , *Friction Stir Welding and Processing IV, Edited by Mishra, Mahoney, Lienert & Jata TMS* (2007), p.29-38.

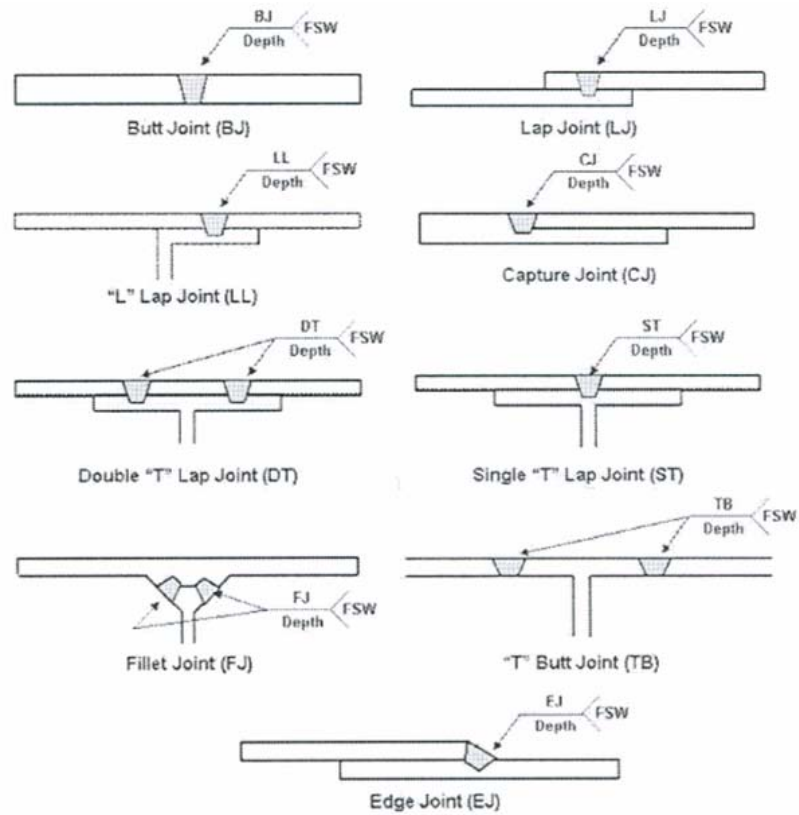


Fig. 1.1. Joint designs possible with FSW [1,2]

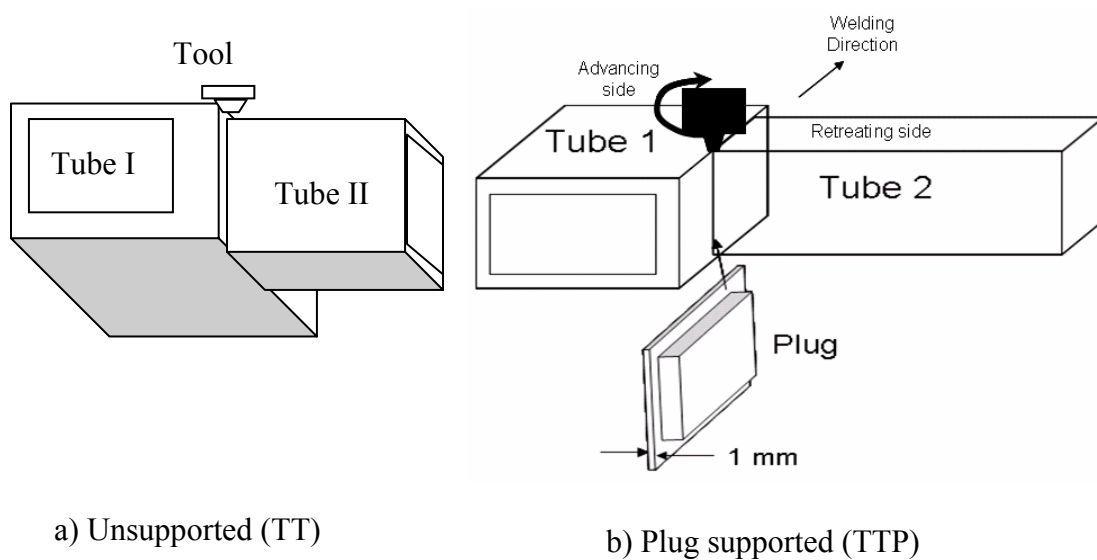


Fig. 1.2. Tube to tube weld configurations

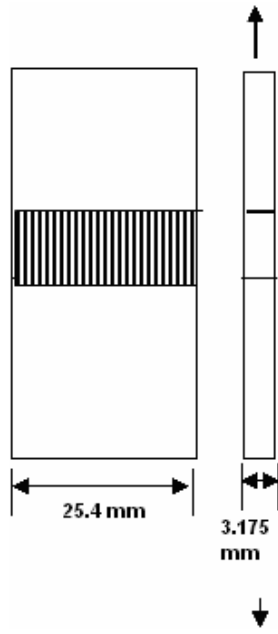
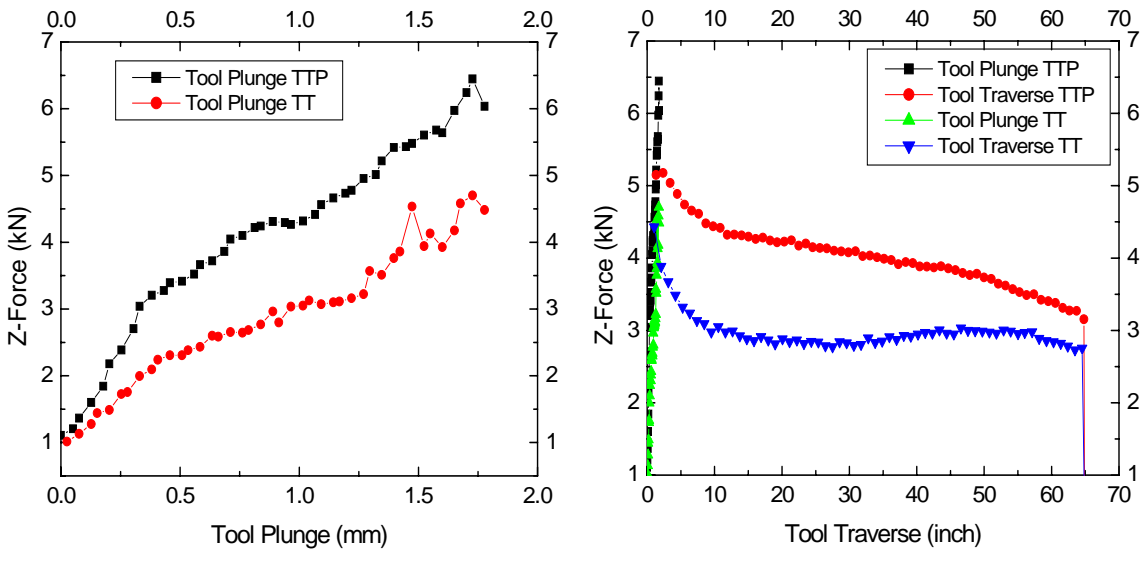
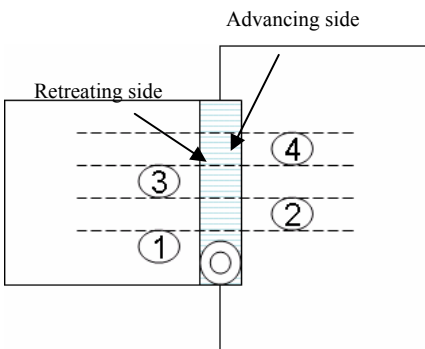


Fig. 1.3. Coupon used for tensile testing



a) Z-forces variation during tool plunge b) Z-forces variation during tool traverse

Fig. 1.4. Plunge forces analysis during tool plunge and traverse



a) Location of samples

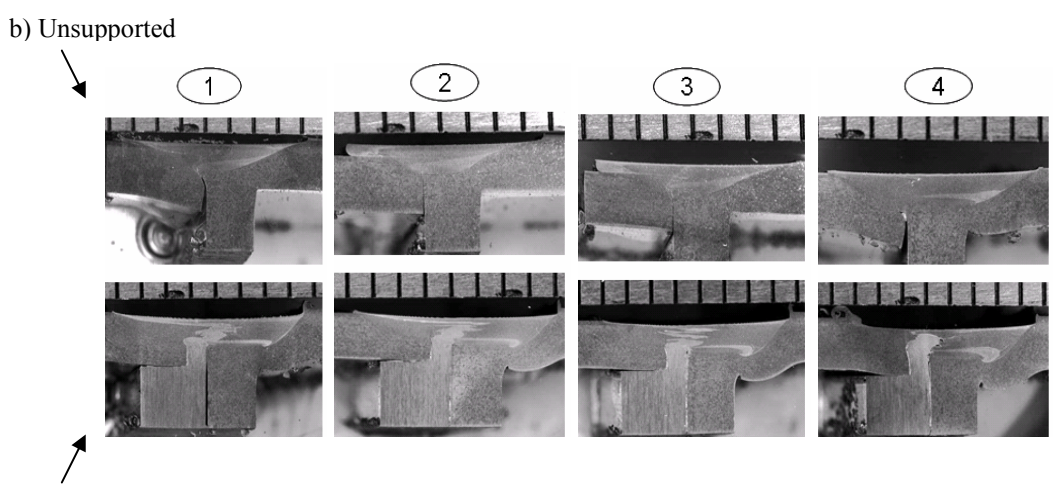


Fig. 1.5. Transverse weld sections along the weld length

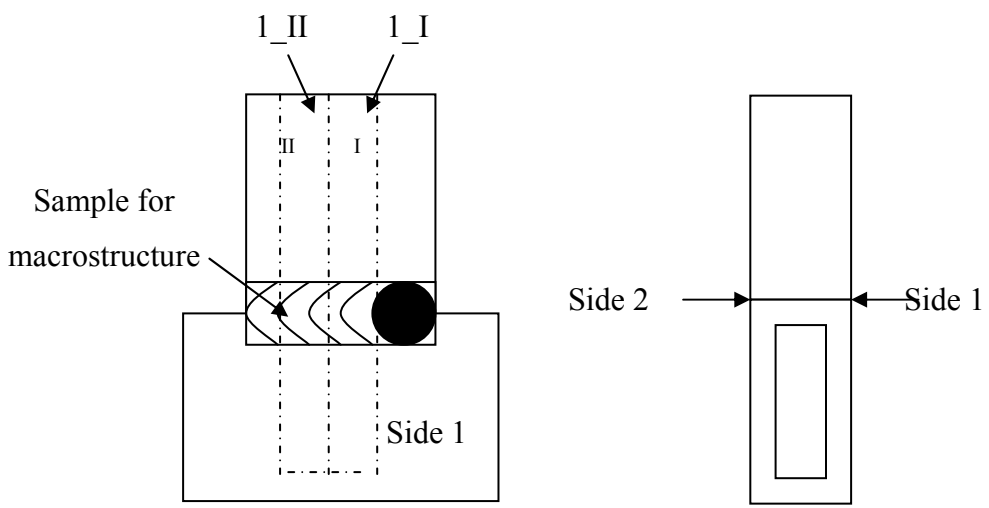
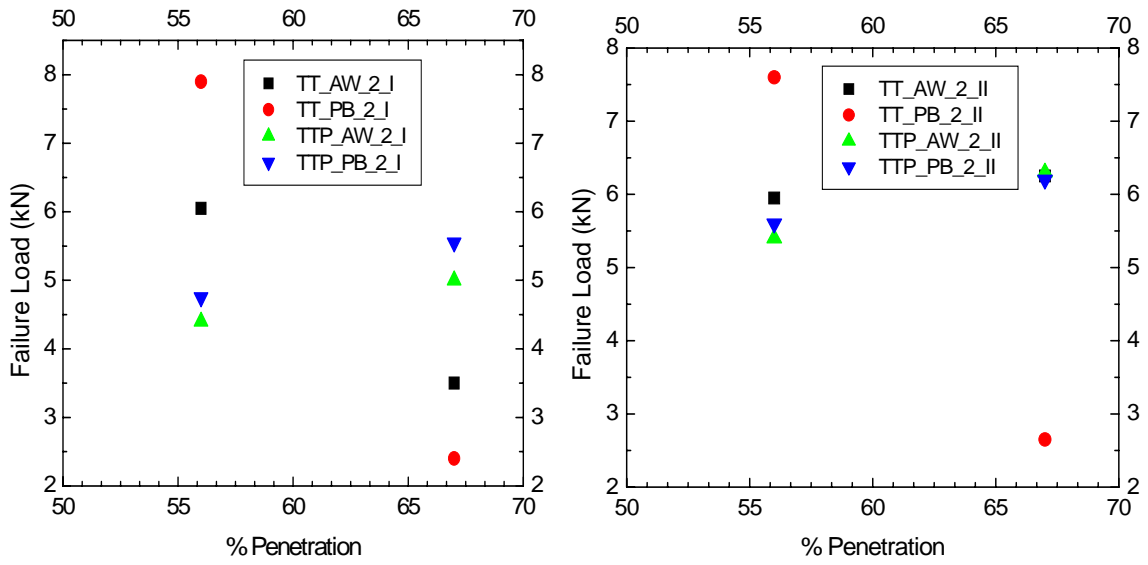
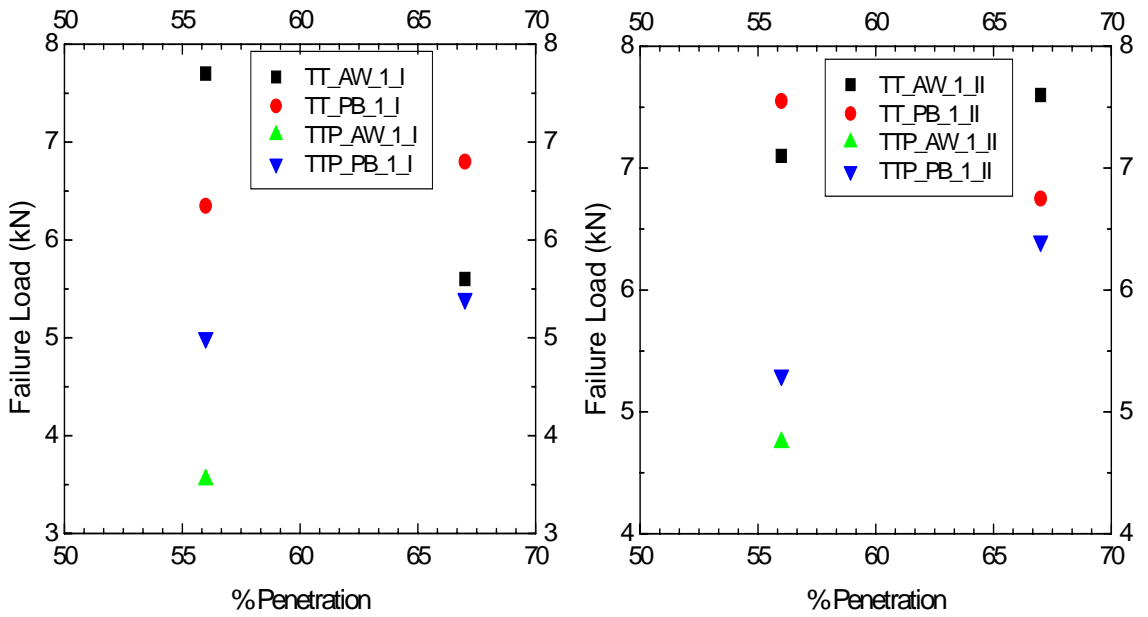


Fig. 1.6. Specimen details for weld categories



a) Sample 2_I

b) Sample 2_II



c) Sample 1_I

d) Sample 1_II

Fig. 1.7. (a-d) Effect of paint bake on failure loads for welds with two different penetration depths

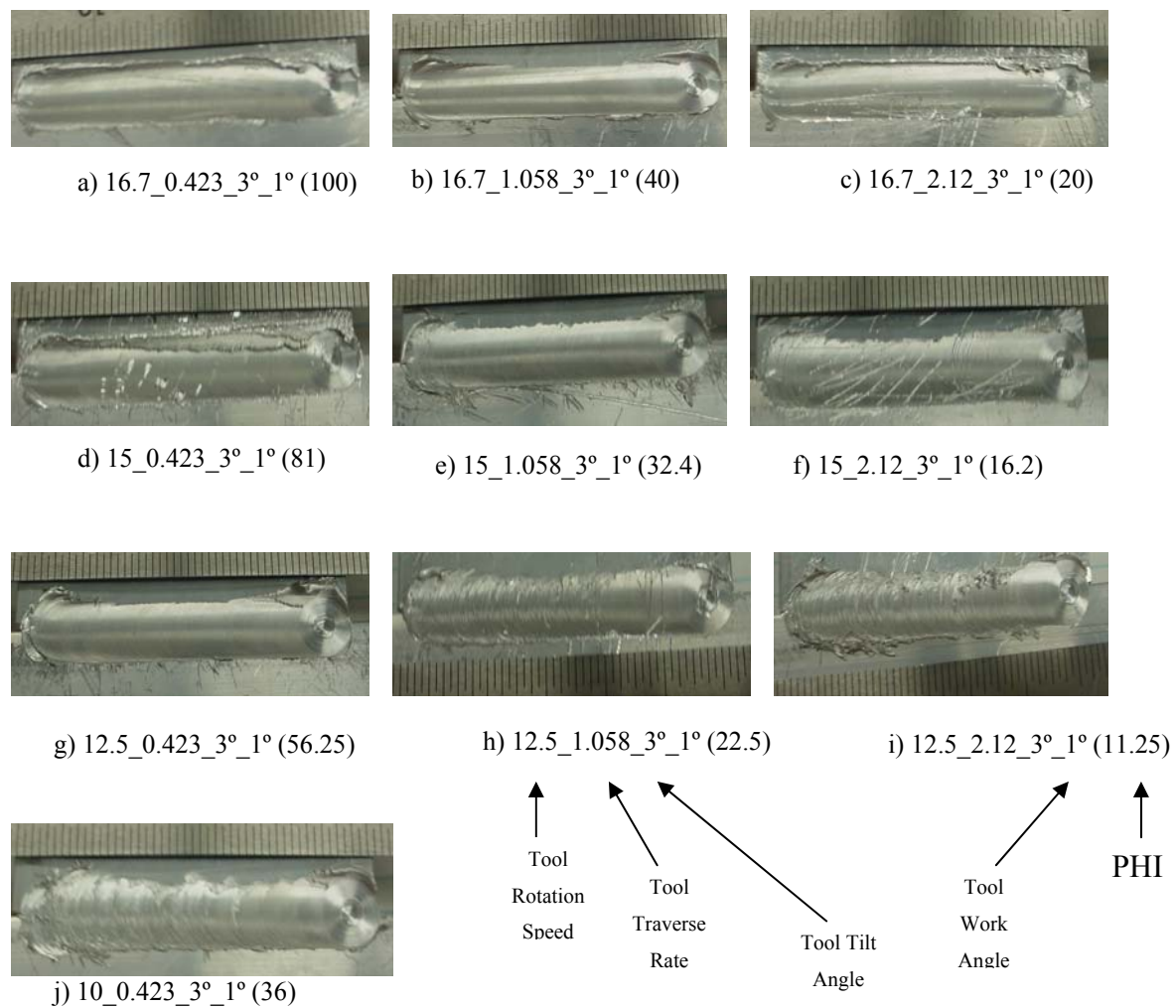


Fig. 1.8. Comparison of weld beads for different process parameters

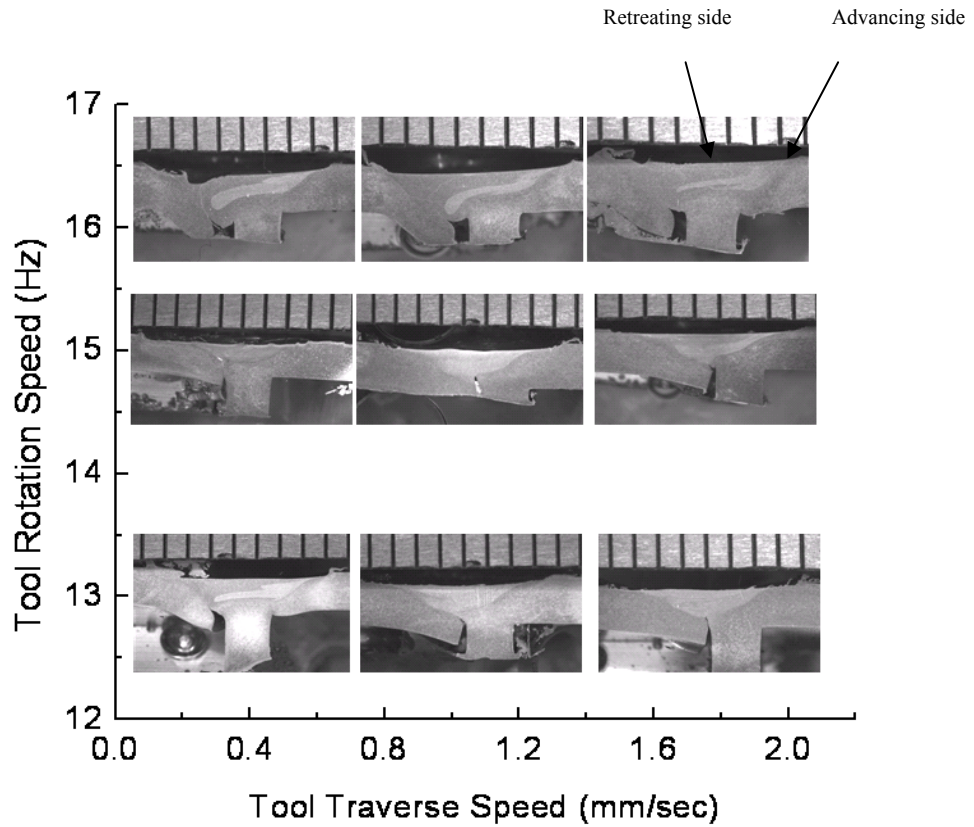


Fig. 1.9. Process map for unsupported tube to tube welds

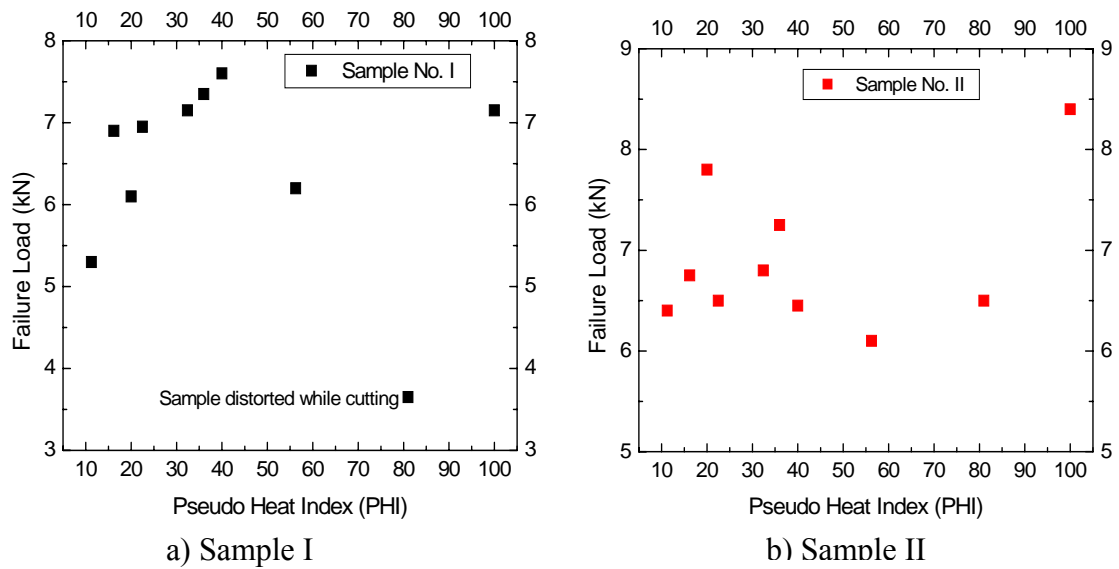


Fig. 1.10. Effect of PHI on tensile properties of unsupported tube to tube welds

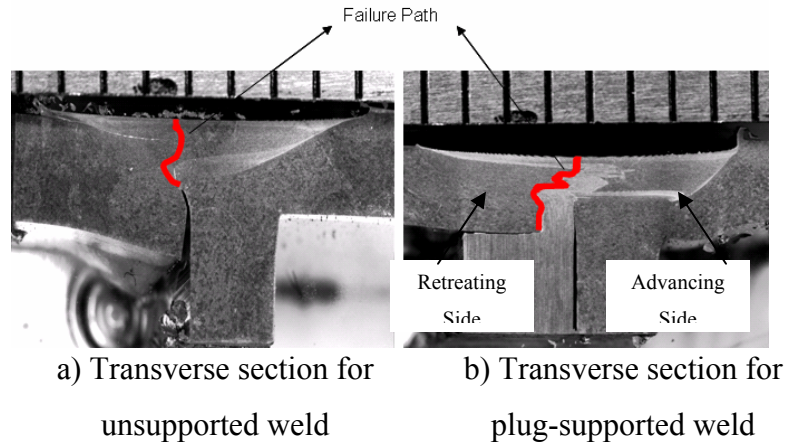


Fig. 1.11. Failure path for a) Unsupported and b) Plug supported tube to tube welds

2. Design of Golf Cart Frame for Friction Stir Welding

Kamini Gupta, Rajiv S. Mishra*

Department of Materials Science and Engineering

Missouri University of Science & Technology

Rolla, MO 65409, USA.

* Corresponding author: Tel.: +01 573 341 6361 fax: +01 573 341 6934

E-mail: rsmishra@mst.edu

(Prepared for submission in MATERIALS AND DESIGN journal)

ABSTRACT

The applicability of friction stir welding (FSW) for the fabrication of built-up structures was explored in this work. The objective was to develop design guidelines for welding of golf car sub-frame by the FSW method. A used Yamaha GE 16 golf cart was considered for analysis. The original frame of the golf cart and the sub-frame for rear suspension were made of circular cross section steel extruded tubes. For the purpose of weight reduction, a new sub-frame was designed using rectangular cross section Al tubing. Selection of Al over steel was done using Ashby's material property charts and material indices. The geometry of the Al tubing was determined on the basis of shape factor calculations and weight saving considerations. Shape factors for torsion and bending loading conditions were determined for the existing material and geometry combination. The rear suspension sub-frame was re-designed for rectangular Al tubes considering space limitations and FSW process constraints with respect to the possible joint designs, tool accessibility concerns, available workbench area on the machine and clamping issues. The finite element analysis (FEA) method was used for estimating the performance of the frame under different ground conditions. The ANSYS 10.0 package was used for modeling and static analysis of the frame. A torsional stiffness parameter was used for the assessment of frame performance.

Keywords: Shape factor, Material index, Finite element analysis (FEA), Torsional stiffness, Material property chart

2.1 INTRODUCTION

Use of aluminum in the automotive industry is increasing to meet the weight reduction targets for the vehicles. Lightweight vehicles perform better with respect to fuel efficiency, safety and emission standards. In order to use aluminum alloys for automotive applications, it is necessary to research alternate joining methods for aluminum alloys. Friction stir welding has developed as a prominent joining method for aluminum alloys. In this work, a design investigation was done for the replacement of a MIG welded steel golf cart frame with a friction stir welded aluminum frame within the same design envelope. Various steps associated in the design of a frame include research, modeling, optimization and testing [1]. Geometric shapes, materials used, loads acting on the frame, deformation modes under different loading types are the research areas that should be particularly explored for frame design. Frame design is a difficult aspect because of several reasons [1]: it must be designed before other systems, it cannot be finalized until other systems are finalized, it is the largest single component, and it must be lightweight and rigid. Basic frame design was not explored much in the present work as the new frame was built on the existing design envelope and most of the components were retained in the new design.

Extruded aluminum tubes were used in place of steel tubes. Young's modulus (E) of aluminum (70 GPa) is one third of the steel (200 GPa). Also, the density (ρ) of aluminum (2700 kg/m³) is one third of that of steel (7800 kg/m³). Therefore, specific stiffness (E/ρ) of aluminum will be equal to that of steel. Equivalent structural performance is attained by the use of specific section sizes and material thickness. A significant weight reduction could be achieved by the replacement of steel with aluminum. Other advantages associated with the usage of aluminum extruded sections are [2]:

- Flexibility in section design
- Possibility of making variety of profile shapes
- Reduction in part count
- Strength to weight ratio is higher than steel
- Extrusion dies are cheaper than stamping dies

Another important step in frame design is to understand the frame deformation under different loading conditions. Primarily there are four deformation types for an automotive chassis [3]:

- a. Vertical bending – Weights of driver and other components mounted on the frame leads to this type of deformation. Bending of the frame would be different under static and dynamic loading conditions.
- b. Lateral bending – Road camber, side wind loads and centrifugal force due to cornering cause lateral bending. Under this deformation mode, the frame is constrained at the tires and sideways forces act along the length of the frame. Lateral forces act in combination with vertical bending of the frame.
- c. Horizontal lozenging – Forward and backward forces applied at the opposite wheels cause this deformation. This loading type distorts the frame into the shape of a parallelogram.
- d. Longitudinal torsion – Torsional loads results from applied loads acting on one or two oppositely opposed corners of the cart. The resulting torsional deformation can affect the performance of vehicle. Resistance to the torsional deformation is defined as torsional stiffness of the frame. Performance of the chassis is primarily assessed in terms of torsional stiffness measured as $\text{kN} - \text{m}$ per degree.

FEA was used for static analysis of frame. The FEA method can provide more accurate data for the structural analysis. Using the FEA method, structural optimization can obtain a more reasonable structure and can make full use of materials. FEA methods are widely used for design optimization of vehicle frames. The frame is confirmed as satisfactory if it meets performance criteria against vertical bending and torsional loadings. FEA was used for the assessment of frame performance under these two loading conditions in this work.

FSW is a solid state joining process [4] that involves plunging and traversing a rotating tool along the weld line. Improved weld quality, low power requirements, no filler material, no shielding gas, and environmental friendliness are some of the significant advantages that FSW has to offer over conventional welding technology. A schematic of FSW is indicated in fig. 2.1. The present structure was assembled using the MIG welding method along with mechanical fastening. The possibility of replacing MIG welds with FSW was explored. It was found that research done to develop different joint designs with FSW was limited to solid structures. FSW of round tubes was done but with an internal support which took care of the downward plunge force. Some work was done on FSW of rectangular tubes without internal support; therefore rectangular tubes were used for the sub-frame.

The Yamaha GE 16 golf cart used for the current analysis is shown in fig. 2.2. The front clip region of the frame is up to 335 mm from the front tube. The load of the steering motor is transmitted to the front clip region. The main cage extends from 335 mm to 1780 mm. Passenger and driver weights are transmitted to the main cage region of the chassis. The rear suspension sub-frame is also mounted in the main cage region. The rear clip region has rear suspension springs and the rear axle. An electric motor is mounted on the rear axle. The rear suspension sub-frame was designed for the friction stir welding (FSW) method. The existing rear suspension sub-frame is shown in fig. 2.3.

2.2 METHODOLOGY

2.2.1 Material Selection

Selection of material for a component is performed based on the purpose the component has to serve. The golf cart frame serves the following important functions:

- Supports and locates drive-train components like suspension parts, transmission parts etc.
- Contributes to the rigidity of the vehicle
- Acts as a mounting bracket for all other components

Weights of all the components mounted on the frame are transmitted to it. It simulates the condition of a simply supported beam subjected to either point load or uniformly distributed load depending on the component placed on it. Material selection was done by assuming each tube of the frame as a simply supported beam. Material indices were calculated aiming for a lightweight, stiff beam. These material indices are then used as x and y axes for the material property chart.

For a beam of fixed length L and free cross section area A as indicated in fig. 2.4, the deflection on application of force F should be less than δ , the maximum allowable deflection. This constraint is translated for the stiffness S of the elastic beam as [5]

$$S = \frac{F}{\delta} \geq \frac{C_1 EI}{L^3} \quad (2.1)$$

where,

C_1 – Constant, depends on the load distribution on the beam

E - Young's Modulus for the beam material (N/m^2)

I - Second moment of area of the beam section (m^4) and is given by,

$$I = \frac{A^2}{12} \quad (2.2)$$

and,

$$A = \frac{m}{L \cdot \rho} \quad (2.3)$$

where,

m – Mass of the beam (kg)

ρ - Density of the beam material (kg/m^3)

Substituting eqns. (2.2) and (2.3) in eqn. (2.1), we get an equation for the weight of the beam as,

$$m \geq \left(\frac{12S}{C_1 L} \right)^{1/2} \cdot (L^3) \cdot \left(\frac{\rho}{E^{1/2}} \right) \quad (2.4)$$

The parameter representing material properties in eqn. (2.4) is $\frac{E^{1/2}}{\rho}$. This is represented as material index M1. For reducing the weight of the frame, the material index M1 should be maximized. CES EduPack 2007 software was used for plotting material index M1 against the density to obtain the material property chart indicated in fig. 2.5a. It was observed that metals, composites and ceramics exhibited higher values of M1. However, considering the fabrication aspect and cost factor, material selection was made from the metals family of materials. The metals family of material property chart is highlighted in fig. 2.5b. Properties for different candidates in the metals family are summarized in Table 2.1. It was observed that Mg-alloys and Al-alloys showed higher values of M1 with comparatively lower densities than Ti-alloys and low alloy steel. FSW was to be used as the joining method for the fabrication of golf cart frame. FSW is primarily explored for the Al-alloys, therefore Al-alloy was chosen as the material for fabrication of the sub-frame of the rear suspension of the golf cart. 6XXX series Al alloys were selected from series of available Al-alloys. 6XXX series Al alloys have yield strength comparable to mild carbon steel and can be readily extruded. They have good weldability and excellent corrosion resistance [6]. Hence, extruded 6061 T6 Al alloy was used with rectangular cross section for the golf cart sub-frame.

Table 2.1. Postscript for material selection

Material	Material Index $M1 = \frac{E^{1/2}}{\rho}$ (GPa^{1/2}/ (kg/m³)) x (1000)^{1/2}	Density, ρ (kg/m³)	Comments
Mg-alloys	0.105	1740-1950	Much research work is not available for joining with FSW
Al-alloys	0.09	2500-2900	Selected for new frame
Ti-alloys	0.063	4400-4800	Material cost is high, joining requires shielding gas atmosphere
Low alloy steel	0.057	7800-7900	Mostly used for structural members. Also used in current frame

2.2.2 Geometry Selection

The existing rear suspension sub-frame was made with circular cross section steel tubes. The frame undergoes a bending load due to the components mounted on the frame. Owing to the motion of the vehicle on uneven surfaces, it is also subjected to twist loads. The current geometry of the frame withstood both the loads satisfactorily without failure. This was clear from the history of golf cart provided by the seller and also there were no signs of repair on the frame. It was concluded that the existing design performed acceptably under both bending and torsional loads.

The mass of the unit length of tube was the primary parameter used for geometry selection. Adherence to the bending and torsional stiffness specification was ranked as the secondary parameter in shape selection. Bending stiffness and torsional stiffness for circular cross section steel tubes were determined. Bending and torsional stiffness numbers for the steel sub-frame were used as bench-marks. It was required that the new frame geometry should meet these specifications. The geometry of the new sub-frame

was estimated using the calculated specification. Bending stiffness and torsional stiffness calculations were performed assuming beam and shaft models for the frame respectively. Feasible geometries of the rectangular Al tubes that satisfied the bending and torsional loading criteria were determined using eqns. (2.8) and (2.13) respectively. Table 2.2 provides summary of tube geometry calculations.

For bending loading, bending stiffness of a beam is given by S,

$$S \propto EI \quad (2.5)$$

where, E-Young's Modulus of beam material (N/m²), and I – second moment of area (m⁴)

For optimum performance against bending load, bending stiffness of the new design should be equal to that of the existing design.

Therefore,
$$S_N \geq S_E \quad (2.6)$$

Under minimum performance condition,

$$S_N = S_E \quad (2.7)$$

or,
$$E_N I_N = E_E I_E \quad (2.8)$$

For a circular hollow tube, second moment of area is given by,

$$I_E = \frac{\pi}{4}(r_o^4 - r_i^4) \quad (2.9)$$

where, r_o - outer radius (m), and r_i - inner radius (m)

For a hollow rectangular tube,

$$I_N = \frac{1}{6}h^3t\left(1 + \frac{3b}{h}\right) \quad (2.10)$$

where, h – height of tube (m), b – width of tube (m), and t – thickness of tube (m)

Subscripts E and N are used for the existing and the new designs respectively.

For torsional loading, torsional stiffness of a shaft is given by S_T ,

$$S_T = \frac{KG}{L} \quad (2.11)$$

where, G – Shear Modulus of the material ($\text{N}\cdot\text{m}^2$), L – Length of the structure (m), and K – Torsional moment of area (m^4)

Under minimum performance condition,

$$S_{TN} = S_{TE} \quad (2.12)$$

There was no change in the length of the shaft only the shape of the shaft was changed.

Therefore, $K_N G_N = K_E G_E$ (2.13)

For existing circular hollow tube, and, for a new hollow rectangular tube,

$$K_E = \frac{\pi}{2}(r_o^4 - r_i^4) \quad (2.14)$$

$$K_N = \frac{2tb^2h^2}{(h+b)}\left(1 - \frac{t}{h}\right)^4 \quad (2.15)$$

Tube sections available in the market were tested for mass, bending and torsional loading criteria, with results shown in Table 2.2. Bending stiffness and torsional stiffness were calculated for the existing geometries. Mass per unit length, bending stiffness and torsional stiffness were determined for the existing steel tube as 3797 gm/m , $32.9 \times 10^6 \text{ GPa}\cdot\text{mm}^4$ and $24.8 \times 10^6 \text{ GPa}\cdot\text{mm}^4$ respectively.

Table 2.2. Geometry selection summary

Sr. No	h mm	b mm	t mm	$I_N \times 10^4 \text{ mm}^4$	$E_N I_N \times 10^6 \text{ Gpa}\cdot\text{mm}^4$ $E_E I_E = 32.9 \times 10^6$	$K_N \times 10^4 \text{ mm}^4$	$K_N G_N \times 10^6 \text{ Gpa}\cdot\text{mm}^4$ $K_E G_E = 24.8 \times 10^6$	Mass / Length gm / m $M_E L_E = 3797$
1	25.4	101.6	3.2	11.27	7.89	19.52	5.07	2092
2	44.5	88.9	3.2	32.53	22.77	55.28	14.37	2202
3	38.1	101.6	3.2	26.34	18.44	48.09	12.50	2312
4	44.5	101.6	3.2	36.52	25.56	65.93	17.14	2422
5	50.8	101.6	3.2	48.56	33.99	85.74	22.29	2532
6	44.5	114.3	3.2	40.50	28.35	76.76	19.96	2642
7	44.5	127.0	3.2	44.48	31.14	87.75	22.82	2862
8	76.2	101.6	3.2	117.07	81.95	180.55	46.94	2972
9	50.8	127.0	3.2	58.97	41.28	114.83	29.86	2972
10	38.1	152.4	3.2	38.05	26.63	79.35	20.63	3192
11	50.8	152.4	3.2	69.37	48.56	144.69	37.62	3412

* The values for existing design are denoted with subscript 'E'

The calculations were performed for 6061-T6 AA, based on commercially available extruded sections

All tube dimensions considered had 3.2 mm wall thickness. Several trial FSW runs were made on rectangular tubes with 3.2 mm wall thickness. This tube wall thickness satisfactorily withstood the downward plunge force. Tube dimensions meeting all three selection criteria are highlighted in Table 2.2. Rectangular tube of 101.6 mm × 50.8 mm with 3.2 mm wall thickness exhibited optimum performance with a 33% weight savings.

2.2.3 Frame Design

The rear suspension sub-frame present on the golf cart is indicated in fig. 2.6a. Hollow circular cross section steel tube was welded to the box. An additional steel tube was welded to the parallel rails on both sides to prevent deformation. The box and tube were welded to the rail by the MIG welding method. A rubber bush was mounted in the box, which acts as a damper. The rear sides of both the rail tubings were bolted to the rear wheel axle. Dimensions on the existing steel sub-frame were measured. Critical dimensions were maintained for the new sub-frame design. Circular steel tube was replaced with rectangular Al tube in the new frame. The new frame design is shown in fig. 2.6b.

Two designs were made for the box where the rubber bushing is mounted. These designs are shown in fig. 2.7 respectively. The boxes were designed for the FSW method. In box design 1, c-channels were used as supporting blocks for 3.175 mm thick top and bottom plates. The thickness of the c-channel was also 3.175 mm. In the second box design, top and bottom plates were supported by 6.35 mm thick plates. Tube I was fixed to the box with the aid of adapters indicated in fig. 2.8. These adapters were machined from 50.8 mm thick Al plates.

2.3 FINITE ELEMENT ANALYSIS

Modeling and analysis of the entire golf cart chassis was done using the ANSYS 10.0 package. The model developed was for the new rear suspension sub-frame in the old chassis. For generating the finite element analysis (FEA) model, all the measurements were taken on the existing frame. The origin was fixed in the front towards the passenger

side of the vehicle. The cartesian co-ordinate system was such that the positive x-axis was directed towards the right along the front lateral member of the chassis; negative y-axis was directed along the rear of the vehicle. The z-axis pointed perpendicular to the x-y plane in the upward direction. Nodes were generated based on the measurements taken on the existing frame. The overall chassis was defined with 71 nodes and 86 elements. Two different types of elements were used in the model. Description of the elements is listed in Table 2.3.

Table 2.3. Elements used for FEM of the golf cart chassis [7]

Elements	Description	Material	Application
BEAM 23 3D Elastic	Uniaxial element with tension-compression and bending capabilities. It has three degrees of freedom at each node	Low alloy steel	Rail members of main frame
		6061 T6 Aluminum	Rail members of rear suspension sub-frame
COMBIN14	Torsional spring-damper option is a purely rotational element with three degrees of freedom at each node:	Spring steel	Rear suspension spring

Frame rail members were defined as 3D Elastic beam elements. Rail members for the main frame were defined as a beam with hollow circular cross section. Elements of the rear suspension sub-frame were defined as a hollow rectangular cross section beam. The rear suspension springs were modeled using COMBIN14 element of ANSYS. The spring constant for the existing spring geometry was calculated using eqn (2.16) [8]

$$K = \frac{G \cdot d^4}{8 \cdot D^3 n} \quad (2.16)$$

where, K is the spring constant (N/m)

G is the modulus of rigidity for the spring material (GPa)

d is the wire diameter (m)

n is the number of active turns in the spring

D is the mean coil diameter (m)

Based on the existing spring geometry, the value of K was calculated as 4.66×10^{-7} N/m. Three different materials were used in generating the entire model. These are listed in Table 2.4. Certain assumptions were made in modeling of the chassis using ANSYS:

- For beam elements the initial strain was assumed to be zero. Each rail member might have some initial strain associated with it depending on the joining method used, prior handling, and ground conditions in transit.
- Masses of some of the parts mounted on the chassis were assumed. Though the exact weight of the golf cart was measured before dismantling as 434 kg, masses of the individual components were not known.
- The second moment of area was defined only about z-axis and was assumed as zero for y-axis.
- FEM was subjected only to linear static analysis.

Table 2.4. Material properties used for FEM

Material	Properties*		
	Density ρ kg/m ³	Young's Modulus E GPa	Poisson's ration ϵ
Low alloy steel	7900	205	0.29
6061 T6 Aluminum	2730	68	0.33
Spring steel	7900	210	0.37

*Material properties were taken from the database of CES Edupack software

Performance of the frame was evaluated against two different ground conditions. Weights of different components mounted on the frame were applied at the mounting points. Applied loads cause the vertical bending deformation of the frame. The four ends where tires were mounted were kept fixed and approximate masses of passenger, driver and seat were applied at four nodes respectively. Weights of the batteries were applied as the boundary condition at the points where the battery frame was welded to the main chassis. The electric motor weight was applied as a point force at the center of the rear axle. Vertical bending experienced by the frame is indicated in fig. 2.9a and fig. 2.9b respectively. Modeling results indicated maximum deformation in the middle part along the chassis length. This region experiences combined vertical bending owing to passengers and mounted batteries. The maximum deformation observed was 1.4mm.

In order to evaluate the torsional stiffness of the chassis, the boundary conditions that were applied to the model are indicated in fig. 2.10b. A torque was applied to the front end of the chassis by applying equal and opposite vertical forces on the driver's side and the passenger's side. The applied torque is defined as [9]

$$T = F \cdot d \quad (2.17)$$

where, d is the lateral distance between the driver and passenger load application points (m) and, F is the applied force (N).

The rear wheels were restrained in all x , y and z translations and rotations. The applied boundary conditions are similar to the constraints applied by a twist fixture used for measuring torsional stiffness of racecars [9]. Torsional stiffness of the frame is determined using eqns. (2.18).

$$K_c = \frac{T}{\phi} = \frac{F \cdot d}{0.5 \cdot (\phi_d + \phi_p)} \quad (2.18)$$

ϕ is the average twist of the chassis due to the applied torque, ϕ_d , is the twist angle of the frame on the driver's side and ϕ_p , is the twist angle of the frame on the passenger's side.

An applied force of 4 kN produced a torque of 3.97 kN – m, where $d = 1$ m was used as the distance between the load application points. Due to the asymmetric nature of the chassis, the deflections were not similar. The twist to which the chassis was subjected was determined as 0.043 on the driver's side and 0.042 on the passenger side. Chassis twists at different nodes were obtained from the results of FEA modeling. The torsional stiffness under a static loading condition for the frame with Al rear suspension sub-frame was calculated as 93.61 kN–m/deg. Fig. 2.10 indicates the deformation of the chassis due to the applied torque. An overall maximum deflection of $\cong 5$ cm was observed on the driver's side in the front suspension region of the vehicle. The outcome of FEA modeling indicated that the current design was satisfactory for the design conditions it was analyzed for. However, no existing standard was found for the design specifications for a golf cart. The loads applied as boundary conditions for vertical bending and torsional loading were approximations. However, a detailed methodology was presented that could be applied for the analysis of any vehicle frame if the design load data is known.

2.4 CONCLUDING REMARKS

This paper addressed several issues associated with frame design considering golf cart geometry. A combined material index representing different material properties was developed considering a beam model. A material property chart was plotted for these material indices to locate different families of materials. Aluminum alloys were selected as the best fit based on the material index, ease of joining by the FSW method and cost criteria. Geometry selection was done considering weight savings, bending and torsional stiffness criteria. Optimized Al rectangular sections exhibited optimum performance with 33% weight savings. An FE model was generated in ANSYS. FEM performed satisfactorily under vertical bending and torsional loading conditions. Torsional stiffness of the frame was calculated as 93.61 kN-m/deg based on the results of finite element analysis. Present work provides an approach for the design of the vehicle frame

considering material selection, geometry selection, and use of FEA methods for assessment of structural performance.

2.5 REFERENCES

1. Brian Auer, Jared McCombs and Edwin Odom, “Design and Optimization of a Formula SAE frame”, *SAE Technical Paper series*, (2006)
2. Dino Triantos and Matthew Michaels, “Design and Fabrication of an Aluminum Engine Cradle for a General Motors Vehicle”, *SAE Technical Paper series*, (1999)
3. William B. Riley and Albert R. George, “Design, Analysis and Testing of a Formula SAE Car Chassis”, *SAE Technical Paper Series*, (2002)
4. R. S. Mishra, M. W. Mahoney, *Friction Stir Welding and Processing*, *ASM International*, 2007
5. Michael F. Ashby, *Materials Selection in Mechanical Design*, Elsevier, Third Edition (2007)
6. J. Randolph Kissell and Robert L. Ferry, *Aluminum Structures – A Guide to their Specifications and Design*, John Wiley & Sons INC., Second Edition (2002)
7. *ANSYS online documentation*
8. http://www.engr.asp.com/doc/etb/mod/stat1/spring/spring_help.html
9. Lonny L. Thompson, Srikanth Raju and E. Harry Law, “Design of a Winston Cup chassis for Torsional stiffness”, *SAE Technical paper series*, (1998)
10. Elliot Brinkworth, Daniel Jaggard, Martin Royds-Jones, Blake Siegler, David Barton, Andrew Deakin and Adam Heppell, “Application of FEA Techniques to a Hybrid Racing Car Chassis Design”, *SAE Technical Paper Series*, (2000)
11. Wenjie Qin and Weili Zheng, “Rigidity and Strength Analysis and Structure Optimization of one Electric Tractor’s Frame Based on FEA”, *SAE Technical Paper Series*, (2007)

12. Anthony G. Grabowski and Arun K. Jaura, “Ford’s PRODIGY Hybrid Electric Vehicle Powertrain Weight Reduction Actions”, *SAE Technical Paper Series*, (2001)
13. Duane Detwiler, Shantaram Ekhande and Mark Kistner, “ *Computer Aided structural Optimization of Automotive Body Structure*”, *SAE Technical Paper Series*, (1996)
14. David J. Andrea and Brett C. Smith, “Automotive Demand, Markets, and Material Selection Processes”, *SAE Technical Paper Series*, (1994)
15. William F. Milliken and Douglas L. Milliken, *Chassis Design – Principles and Analysis, Based on previously unpublished technical notes by Maurice Olley*, *SAE International*, (2002)

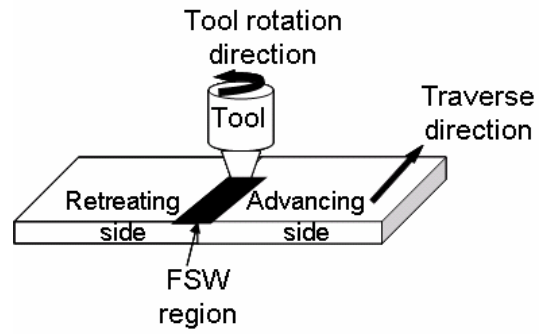


Fig. 2.1. Schematic representation of FSW



Fig. 2.2. Yamaha GE 16 Golf cart

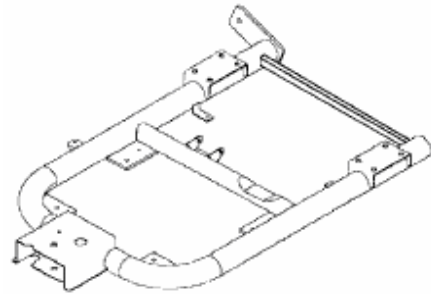


Fig. 2.3. Rear suspension sub-frame

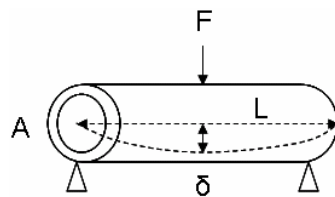


Fig. 2.4. Beam model for material index calculation

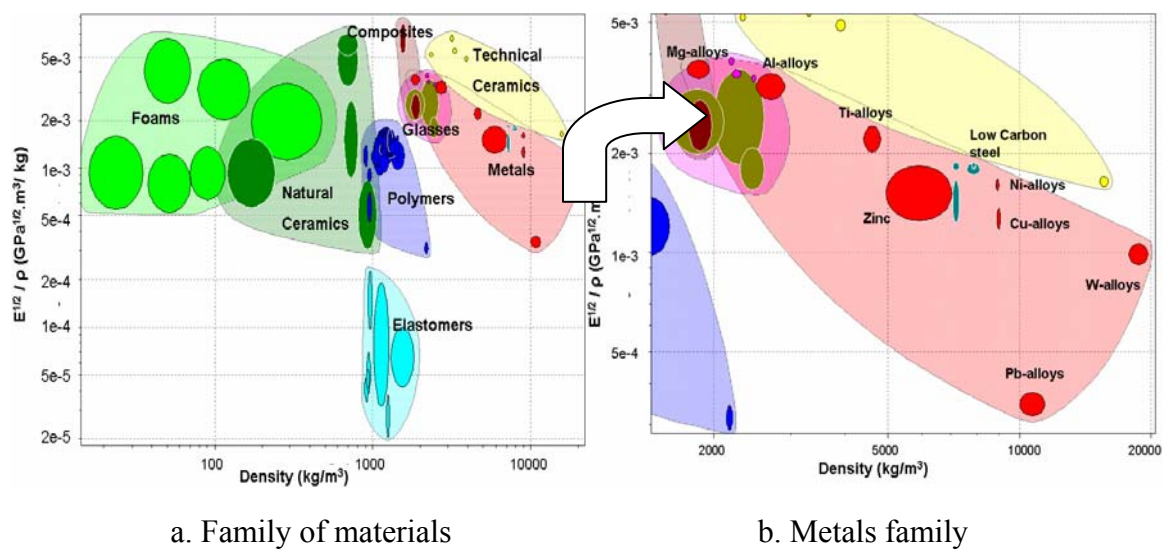


Fig. 2.5. Material selection chart, $E^{1/2}/\rho$ vs. Density (ρ)

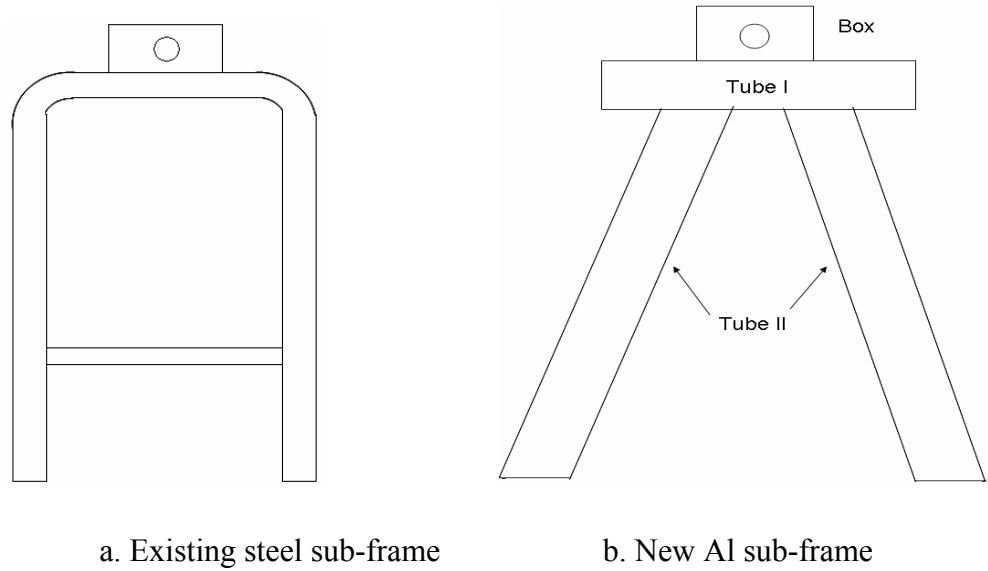


Fig. 2.6. Rear suspension sub-frame designs

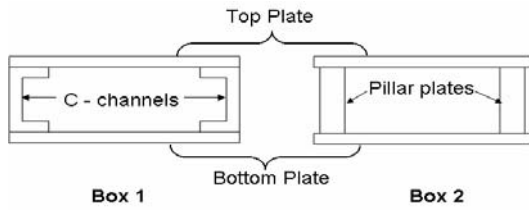


Fig. 2.7. Box designs for new sub-frame

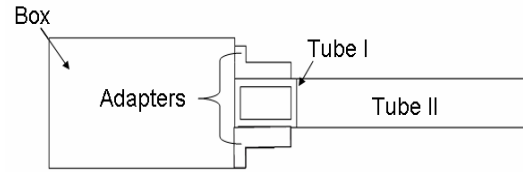
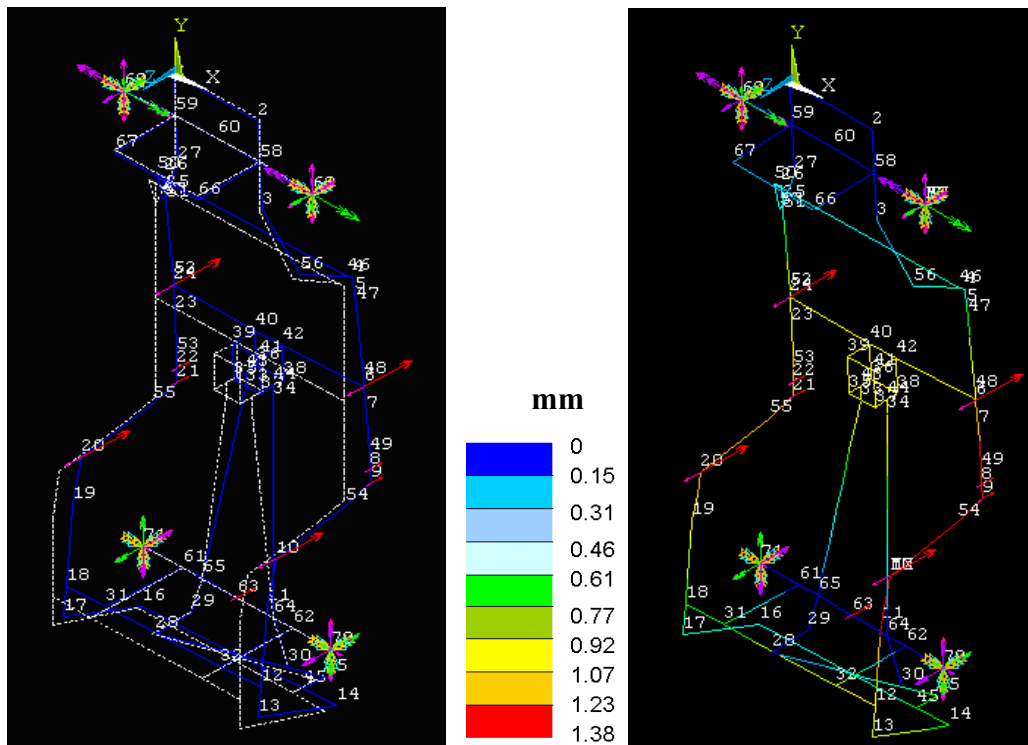


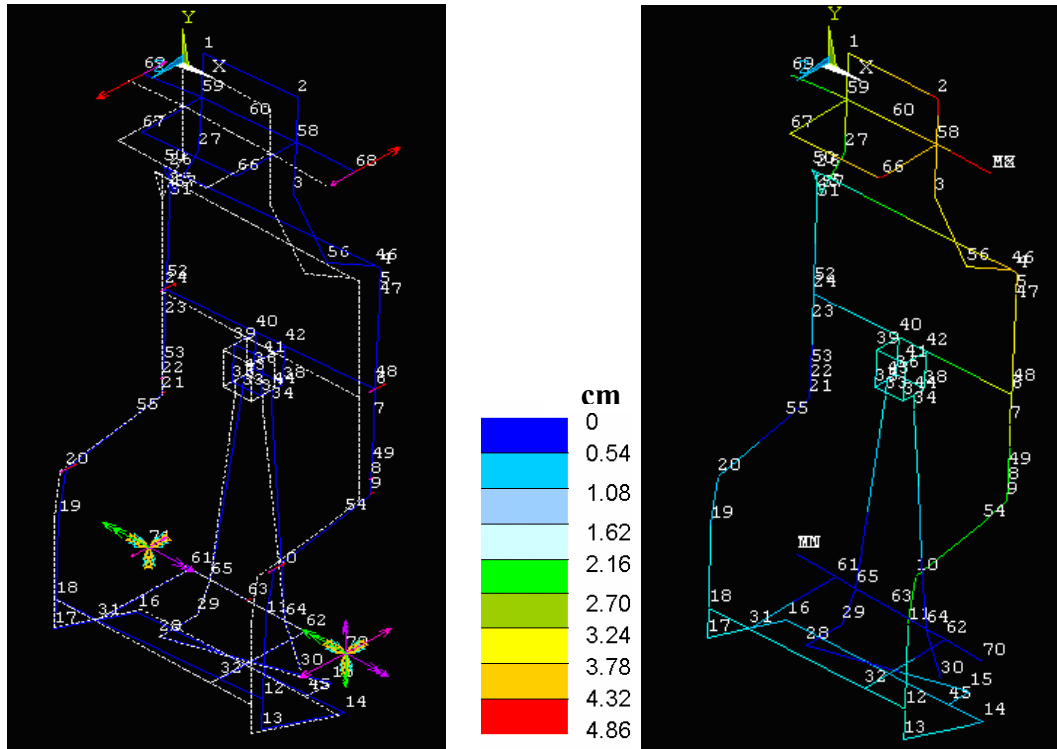
Fig. 2.8. Assembly of box and tube I



a. Deformed (blue) and undeformed (white) frame

b. Degree of displacement vector sum

Fig. 2.9. FEA results for vertical bending deformation mode



a. Deformed (blue) and undeformed (white) frame b. Degree of displacement vector sum

Fig. 2.10. FEA results for torsional deformation mode

VITA

Kamini Ashokkumar Gupta was born on 20th August, 1982, in Nagpur, India. She received her Bachelor degree in Metallurgical engineering from Visvesvaraya National Institute of Technology (VNIT) in May 2004. She served Tata Motors Ltd, Pune from July 2004 to July 2006 as a Supplier Quality Improvement Engineer. She came to USA in August 2006 for pursuing her masters. She graduated from Missouri University of Science and Technology (MS&T), USA in July 2008 with her Masters degree in Materials Science and Engineering.